Assen Zlatarov University
Burgas, Bulgaria

ANNUAL

1

VOLUME LIII, BOOK 1, 2024

TECHNICAL AND NATURAL SCIENCES

ASSEN ZLATAROV UNIVERSITY
BURGAS, BULGARIA

ANNUAL

Vol. LIII, BOOK 1, 2024

TECHNICAL AND NATURAL SCIENCES

Assen Zlatarov University

Assen Zlatarov University
Annual, Vol. LIII, Book 1, 2024
Burgas 8010, Bulgaria
ISSN 2603-3968

ASSEN ZLATAROV UNIVERSITY
BURGAS, BULGARIA

ANNUAL

Annual, Vol. LIII, Book 1, 2024

TECHNICAL AND NATURAL SCIENCES

BURGAS ● 2024

VOLUME LIII. CONTENTS

ANNUAL OF ASSEN ZLATAROV UNIVERSITY, BURGAS
BULGARIA, 2024, v. LIII(1)

OVERVIEW OF CELLULAR SIGNAL MOLECULE BINDING WITH BASIC RECEPTOR TYPES

Dimitar Penev, Petia Tzvetkova
Email: mitkopenev97@gmail.com

ABSTRACT

This article will present a summary of new discoveries which manifest the mechanisms of cellular communications, as well as the potential clinical application that the knowledge of cellular communication mechanisms might bring to certain pathological states.

***Keywords**: cellular signal, mechanism, receptors, cell*

INTRODUCTION

Cells are in a constant state of communication with the outside world and with one another receiving and interpreting millions of signals at a time.

Cells communicate with the external environment through one of the following mechanisms: autocrine secretion, which consists of a cell secreting certain proteins that affect the secreting cell; paracrine secretion, in which the cell exocytosis products affect different cells in the surrounding environment; and endocrine secretion, in which a specific cell secretes products directly into the peripheral blood, which then travel long distances and bind to cells far away from the original cell [1].

Synaptic transmission is another form of cell communication and can be explained basically through the excitatory action of an action potential which stimulates the secretion of neurotransmitters from the presynaptic neurone, which then traverse the synaptic cleft and dock with the postsynaptic neurone, thus propagating the stimulating signal along the neuronal chain [2].

REVIEW OF MECHANISMS

To further expand on the introductory statements regarding cell ligands and target cell receptors, a distinction should be made between the different types of cell receptors and their specific chemical composition.

Cell receptors can be classified into five different categories [3], based on the mechanism through which they achieve signal transduction.

Ligand gated ion channels are integral membrane proteins which are located on the outer surface of the cellular membrane. Once they bind with a specific ligand, they undergo conformational changes that increase the permeability of ions for the cell. They are most often found in cells that are electrophysiologically active, such as cells of the myocardium and neurons.

An example of a specific ligand gated ion channel receptor is the GABA receptors found in the central nervous system of vertebrates.

This is an ionotropic [4] channel receptor, meaning that the opening and closing of the specific ion channel is controlled by the binding of the ligand with the proteins of the channel: if the receptor is not bound the channel won't be open and vice versa. They can be subdivided into two different classes: $GABA_A$ and $GABA_B$ receptors, each of which has a different chemical structure, being composed of different numbers of subunits. The number and chemical composition of each subunit affects the electrophysiological conductance of the overall receptor [4].

The specific compound that binds with the GABA receptor is γ-Aminobutyric acid, one of the main inhibitory neurotransmitters in the nervous system and brain of mammals [4].

G-protein coupled receptors consist of a cell surface receptor that binds the ligand and a transmembrane protein, G protein.

The G protein consists of seven subunits that pierce the cell membrane several times and undergo structural changes which in turn can activate or inactivate intracellular pathways: enzyme expression and activation, channel opening and closing, etc.

G-protein coupled receptor mechanism can be simplified to a sequence of several steps, which, depending on the type of ligand and its specific receptor, will lead to the activation of different intracellular proteins and their further biochemical reactions.

The first step of the G-protein coupled receptor reaction can be explained simply as the binding of the ligand to the outer cell surface receptor. Once the ligand is bound, the G-protein undergoes a structural change and the bound GDP is phosphorylated to GTP with subsequent activation of the regulatory enzyme that is attached to it [4].

There are many regulatory enzymes that participate in the signal transduction pathway but the most common is adenyl cyclase [5]. Its purpose is to activate the so-called secondary messenger molecules.

Secondary messenger molecules have the function of activating protein kinases, which are specific cellular enzymes that activate cellular proteins through their phosphorylation. Once phosphorylated, the cell proteins are then subjected to export for use in some other locations or for the cell's own needs.

The most studied secondary messenger molecule in signal transduction and cellular communication in general is cyclic adenosine monophosphate (cyclic AMP) [6].

The main function of cyclic AMP is to assist in the phosphorylation of certain cell proteins in conjunction with protein kinase, mostly protein kinase A.

Protein kinase A is composed of four different subunits, two of which have a regulatory function and two of which have a catalytic function [7]. The different subunits of protein kinase A are in a harmonious relationship. If not bound to a cAMP molecule, the regulatory subunits inhibit the functions of the other two catalytic units. On the other hand, if the enzyme is bound to a protein kinase A, the inhibitory effect of the regulatory subunits is removed and the catalytic subunits are free to catalyze a given reaction.

Catalytic receptors are also transmembrane proteins that are usually enzymes or take part in an enzyme complex.

Once a ligand is bound to a catalytic receptor, the receptor is activated and leads to changes in the activity of enzymes on the cytoplasmic side of the cell.

An example of a catalytic receptor is guanylyl cyclase, which is a receptor that accepts specific peptide proteins, some of which are located in the heart and the brain: the atrial natriuretic peptide hormone and brain natriuretic peptide hormone, respectively [8].

The function of atrial natriuretic peptide hormone is to increase vasodilation in vessels of the heart along with heart smooth muscle relaxation [8]. Excretion of Na+ ions in urine is also increased.

The receptor for atrial natriuretic peptide hormone is a transmembrane protein made up of a single segment spanning the entirety of the cell membrane and a short, extracellular chain that binds the peptide.

On binding the hormone, certain structural changes happen and guanosine triphosphate (GTP) is converted to cyclic guanosine monophosphate (cGMP), which then activates a specific kinase, cGMP-dependent kinase. cGMP phosphorylates proteins that have an effect on many bodily structures, such as the medullary renal tubules, lead to activation of certain Na^+ channels [8].

Nuclear receptors are receptors that are found inside the cellular nucleus. Steroid and thyroid hormones enter the cell through a variety of mechanisms, mostly crossing the cell membrane as they are lipid soluble and then binding to the given receptor.

Apart from steroid and thyroid hormones, there are a myriad of other substances that activate these receptors: vitamin D, retinol and thyroid hormone [9].

Nuclear receptors can be classified into two basic types: receptors for steroid hormones, among which are the androgens, glucocorticoids, progesterone and oestrogens, and mineralocorticoids, and receptors for other hormones.

Furthermore, nuclear receptors also bind xenobiotics, substances that are foreign to the organism and thus play a key role in the metabolism of pharmacological drug products through the expression of certain enzymes and proteins that take part in that specific drug metabolic pathway [9].

The basic chemical structure of nuclear receptors can be described as containing five or six domains, each of which serves a specific function: one is for hormone binding, another is for binding DNA, domains for transactivation of DNA and others, respectively [9].

Transactivation is the process through which structural changes are made in a specific region of the DNA molecule ,which leads to transcription of specific products and their subsequent translation.

Nuclear receptors are found in various different concentrations in the cell nucleus and in the tissue and their response to a given ligand depends on their number in a given cell [10].

In this review, a comparison between the various pathological states that can be associated with the above-mentioned structures is discussed.

GABA receptors have been linked to several diseases of the nervous system in humans. Structural mutations in the genes encoding different subunits of the GABA receptors have shown that this leads to problems in the electrophysiological function of the channel.

These mutations have different effects on different parts of the channel and this is dependent on the various types of mutations, their location in the given gene, the affected region of the encoded protein, the subunit gene and the affected gene itself.

Alterations in GABA receptors caused by the above-stated genetic mutations have been linked to idiopathic epilepsy due to changed channel gating characteristics [11].

A more specific example of this is Dravet syndrome, a variant form of epilepsy that affects children starting from the age of 1, which has been linked with gene defects in the genes encoding the A1, B1, B2 and Y2 subunits.

Nuclear receptors and atrial natriuretic peptide hormones have been linked as biomarkers of heart failure in patients suffering from this disease.

Natriuretic peptides have been classified into four different types: A, B, C, and D, with each peptide being secreted from certain tissues in the body. The A peptide was the first discovered and was found in the atria of the heart muscle [11].

Its main function from a physiological point of view is to lead to an increase in vasodilation and an overall branching antihypertensive effect in the body. Additionally, this peptide leads to an increase in natriuresis and diuresis [11].

B-type natriuretic peptide hormone was found to be secreted mostly from the left ventricle of the heart as a result of increased cardiomyocyte stretch which is secondary to increased left ventricular chamber pressure [12].

Additional peptide hormones were discovered in the central nervous system and in the venom of the green mamba snake [12], the names of these peptides being C-type peptide hormone and D-type peptide hormone (D from dendroaspis).

The D-type peptide hormone was shown to have an effect on the relaxation potential of contracted muscle cells in the walls of coronary arteries and the aorta in rodents [12].

The molecular mechanism through which the peptide hormones function is as follows: they bind to specific transmembrane receptors that are located throughout the tissues of the organism, mostly in the kidney parenchyme, endothelium of the vasculature, adrenal glands and in the central nervous system. The names of these receptors are respectively A, B, and C [12].

Once bound, this leads to an increased intracellular production of cyclic guanosine monophosphate (cGMP), which joins the secondary messenger pathway and activates certain protein kinases.

Mutations in G-proteins can lead to a multitude of pathologies in humans, which include retinosis pigmentosa, hyperthyroidism and hypothyroidism, nephrogenic diabetes insipidus, fertility disorders and certain cancers [13]

Retinosis pigmentosa is a genetic disorder that is characterized by intense vision loss and potential blindness as a result of the loss of photoreceptor cells and retinal cell degeneration. The initial stages of the disease start with progressive loss of rod cells, leading to visual field restriction and loss of night vision.

Once the rod cells are fully depleted, death of cone cells is to follow.

Rhodopsin is one of the G-protein coupled receptors involved in the process of vision, its purpose being to dephosphorylate GTP into GDP and then activate a specific enzyme, phosphodiesterase, which has the function of hydrolyzing cGMP at a later point of time [15].

CONCLUSION

Cell receptors and their respective ligand molecules are an elegant and efficient method of achieving communication with the external environment and with other cells in the organism.

It is important to understand their mechanism and function as this proves beneficial in the understanding of the pathogenesis and progression of certain disease processes.

REFERENCES

1. Kumar, Abbas, Aster, Robbins and Cotran: *Pathologic Basis of Disease*, 10th edition, Elsevier, 2021, p. 17.
2. Boron, Boulpaep et al., *Medical Physiology*, 3rd edition, Elsevier, 2017, p. 307.
3. Boron, Boulpaep et al, *Medical Physiology*, 3rd edition, Elsevier, 2017, p. 47.

4. Sallard, E., Letourneur, D., Legendre, P. Electrophysiology of ionotropic GABA receptors. *Cell. Mol. Life Sci.*, **78** (2021), pp. 5341-5370, https://doi.org/10.1007/s00018-021-03846-2
5. Blumenfield Hal M.D, *Neuroanatomy through clinical cases*, 2nd edition, Sinauers Associates Inc. 2010, p. 20.
6. Vitanova, L., R. Garchev, *Human Physiology*, 3rd edition, Arso, 2020, p. 26.
7. Vitanova, L., R. Garchev, *Human Physiology*, 3rd edition, Arso, 2020, p. 27.
8. Vitanova, L., R. Garchev, *Human Physiology*, 3rd edition, Arso, 2020, p. 29.
9. Boron, Boulpaep et al, *Medical Physiology*, 3rd Edition, Elsevier, 2017, p. 66.
10. Boron, Boulpaep et al, *Medical Physiology*, 3rd Edition, Elsevier, 2017, p. 71.
11. Ghit A, Assal D, Al-Shami AS, Hussein DEE. GABAA receptors: structure, function, pharmacology, and related disorders. *J Genet Eng Biotechnol.*, **19**, 1, (2021), p. 123. doi: 10.1186/s43141-021-00224-0.
12. McDonagh A. Theresa et al, *Oxford Textbook of Heart Failure*, Oxford University Press, 2011, p. 144.
13. Schöneberg T, Schulz A, Biebermann H, Hermsdorf T, Römpler H, Sangkuhl K. Mutant G-protein-coupled receptors as a cause of human diseases. *Pharmacol. Ther.*. **104**, 3, (2004), pp. 173-206. doi: 10.1016/j.pharmthera.2004.08. 008.
14. Kumar, Abbas, Aster, Robbins and Cotran, *Pathologic Basis of Disease*, 10th edition, Elsevier, 2021, p. 1324.
15. Liu, W.; Liu, S.; Li, P.; Yao, K. Retinitis Pigmentosa: Progress in Molecular Pathology and Biotherapeutical Strategies. *Int. J. Mol. Sci.*, **23**, (2022), p. 4883, https://doi.org/10.3390/ijms 23094883.

ANNUAL OF ASSEN ZLATAROV UNIVERSITY, BURGAS
BULGARIA, 2024, v. LIII(1)

IMPACT OF BEE POLLEN AND ROYAL JELLY ON THE GROWTH OF VARIOUS BACTERIAL AND YEAST SPECIES

Ruska Nenkova, Galina Yordanova, Galina Grigorova
E-mail: rdnenkova@abv.bg

ABSTRACT

The impact of bee pollen and royal jelly on bacteria and yeast was investigated separately and in a 1:1 ratio, across various concentrations: 200, 100, 50, 25, 12.5, and 6.25 mg/mL. *It was found that the natural preservatives used inhibit bacteria and yeast to varying degrees depending on their concentrations. Individually, bee pollen and royal jelly exhibit a stronger effect on the selected yeast species, while their combination has a more pronounced impact on the chosen bacterial species. These findings could be valuable for the food and pharmaceutical industries in combating microorganisms and preserving products.*

Key words: *bee pollen, royal jelly, bacteria, yeast, preservatives*

INTRODUCTION

Following the EU regulation, preservatives are food additives that protect against the action of microorganisms (fungi and/or bacteria) and thereby extend the shelf life of foodstuff. The inhibitory effect of preservatives varies, depending on the concentration and type of preservative and the species of microorganism. In recent years, there has been an increasing demand for natural preservatives that not only extend the shelf life but also enhance the quality of products.

Bee pollen contain a wide range of phenolic compounds, proteins, amino acids, carbohydrates, lipids and fatty acids, enzymes, coenzymes, vitamins and bio-elements [1, 2]. Phenolics show antimicrobial activity on pathogenic bacteria and fungi through disrupting their cytoplasmic membranes [3–5]. Kasim Roba Jilo [6] reported that bee collected pollen had high antimicrobial effects against both Gram-negative and Gram-positive bacteria, however; high inhibition differs from species to species, working concentrations, and exposure periods. *E. coli* and *S. boydii* were more inhibited by ethanolic extract than aqueous extract and similar results that different extracts exhibited different antibacterial activities were reported [7].

Another important bee product is royal jelly. Royal jelly is secreted by the hypopharyngeal glands of young worker (nurse) bees, to feed young larva and the adult queen bee [8]. It has been mentioned that the royal jelly has antibiotic activity due to a high concentration of l0-hydroxydecanoic acid in the jelly [9]. Antibiotic effects of royal jelly have been determined against pathogenic bacteria such as *Salmonella, Escherichia coli, Micrococcus pyrogens, Proteus, Staphylococcus aureus,* and *Bacillus subtilis* [9-11].

The aim of this study was to determine the inhibition properties of bee pollen extracts and royal jelly on ten bacterial species and five yeast species, highlighting their potential as natural preservatives in the food and pharmaceutical industries due to their antimicrobial activity.

MATERIAL AND METHODS

Microorganisms:

The microorganisms used in the experiments were as follows: bacteria – *Bacillus subtilis*, *Bacillus thuringiensis*, *Brevibacterium flavum*, *Bacillus pumilus*, *Escherichia coli*, *Pseudomonas fluorescens*, *Pseudomonas aeruginosa*, *Micrococcus* spp., *Sarcina* spp., and *Staphylococcus aureus*. The following yeast species were also used – *Saccharomyces cerevisiae*, *Candida tropicalis*, *Candida utilis*, *Rhodotorula rubra*, and *Trichosporon cutaneum*. These microorganisms are stored at 4°C in the Microorganism Bank of the Department of Biotechnology, Prof. Assen Zlatarov University, Burgas. The nutrient media used for the experiments were: beer wort and beer agar, which were supplied by a brewery, as well as MPB and MPA – media for bacteria.

Methods:

Sample preparation

Fresh bee pollen was collected from Burgas region. The samples were kept in a dry place and

stored at 4 °C before the tests. The ethanolic extracts were prepared by extracting 2 grams of homogenized sample in 10 mL of ethanol (>96%, Merck, Germany) in the dark at room temperature for 7 days [12]. Then the samples were filtered and used for preparation of serial dilutions.

Agar diffusion method by Bauer-Kirby

The serial dilutions of the samples (200, 100, 50, 25, 12.50 and 6.25 mg/mL) of bee pollen and royal jelly were prepared in ethanol. Approximately 20 cm³ of molten Beer Agar was poured into Petri dishes. After cooling at room temperature, 1 cm³ of a cell suspension containing 2-10^9 cells/cm³ was spread over the solid culture medium. Uniform wells were drilled into the inoculated agar medium using a sterile borer, spaced equally apart. In each well, 0.1 cm³ of each concentration of bee pollen and royal jelly were added, respectively. The prepared Petri dishes were incubated in a thermostat at 28-30°C for 48h to allow the microbial culture to develop. The plates were observed for the presence of inhibition zones around the wells and the diameter of inhibition zones was measured. Ethanol was used as negative control.

RESULTS AND DISCUSSION

The effect of bee pollen or royal jelly in varying concentrations: 200, 100, 50, 25, 12.5, and 6.25 mg/mL on ten bacterial species and five yeast species was investigated. It was found out that bacterial growth was dense in most Petri dishes across the different concentrations. Table 1 presents the results of the impact of bee pollen on the growth of the selected bacteria. It can be seen that *Bacillus subtilis*, *Bacillus thuringiensis*, *Escherichia coli*, and *Sarcina* spp. exhibited zones of inhibition at higher preservative concentrations.

In Table 2, the effect of bee pollen on selected yeasts: *Saccharomyces cerevisiae*, *Candida utilis*, *Rhodotorula rubra* and *Trichosporon cutaneum* is shown. Unlike in bacteria, yeast species exhibited zones of inhibition even at lower preservative concentrations.

Table 1. Zones of inhibition in bacteria at different concentrations of bee pollen (mm)

Concentration, µl	B. subtilis	B. thuringiensis	Brevibacterium flavum	B. pumilus	E. coli	P. fluorescens	P. aeruginosa	Micrococcus spp.	Sarcina spp.	S. aureus
200	20	10	-	-	20	-	-	-	20	-
100	20	-	-	-	15	-	-	-	-	-
50	-	-	-	-	15	-	-	-	-	-
25	-	-	-	-	15	-	-	-	-	-
12.5	-	-	-	-	-	-	-	-	-	-
6.25	-	-	-	-	-	-	-	-	-	-
Control sample	-	-	-	-	-	-	-	-	-	-

Control sample – 95% ethanol

Table 2. Zones of inhibition in yeasts at different concentrations of bee pollen (mm)

Concentration, µl	S. cerevisiae	C. tropicalis	C. utilis	R. rubra	T. cutaneum
200	14	-	19	15	7
100	6	-	11	10	7
50	5	-	11	10	5
25	5	-	10	10	5
12.5	5	-	10	10	5
6.25	5	-	10	10	5
Control sample	-	-	-	-	-

Control sample – 95% ethanol

In the following Tables 3 and 4, the results of the effect of royal jelly on the growth of the same bacteria and yeast species are presented. Table 3 shows zones of inhibition in different bacterial species compared to Table 1, specifically in *Brevibacterium flavum, Escherichia coli, Pseudomonas aeruginosa, Micrococcus spp., Sarcina spp.*, and *Staphylococcus aureus*. A similar result to

that in Table 1 was observed only for *Escherichia coli*.

Table 3. Zones of inhibition in bacteria at different concentrations of royal jelly (mm)

Concentration, µl	B. subtilis	B. thuringiensis	Brevibacterium flavum	B. pumilus	E. coli	P. fluorescens	P. aeruginosa	Micrococcus spp.	Sarcina spp.	S. aureus
200	-	-	24	-	18	-	10	10	15	20
100	-	-	15	-	16	-	10	-	10	10
50	-	-	10	-	14	-	10	-	10	10
25	-	-	10	-	-	-	9	-	-	-
12.5	-	-	10	-	-	-	5	-	-	-
6.25	-	-	-	-	-	-		-	-	-
Control sample	-	-	-	-	-	-	-	-	-	-

Control sample – 95% ethanol

Table 4. Zones of inhibition in yeasts at different concentrations of royal jelly (mm)

Concentration, µl	S. cerevisiae	C. tropicalis	C. utilis	R. rubra	T. cutaneum
200	19	-	20	15	15
100	10	-	20	15	15
50	5	-	18	5	15
25	5	-	11	5	10
12.5	5	-	11	5	7
6.25	5	-	10	5	2
Control sample	-	-	-	-	-

Control sample – 95% ethanol

Table 4 again demonstrates similar results for the yeasts *Saccharomyces cerevisiae, Candida utilis, Rhodotorula rubra* and *Trichosporon cutaneum*. Zones of inhibition were formed for all concentrations of royal jelly, as observed with bee pollen.

The obtained results indicate that the strongest effect of bee pollen and royal jelly is on the yeasts at various selected concentrations. This is visually represented with images of the Petri dishes in Fig. 1, 2 and 3.

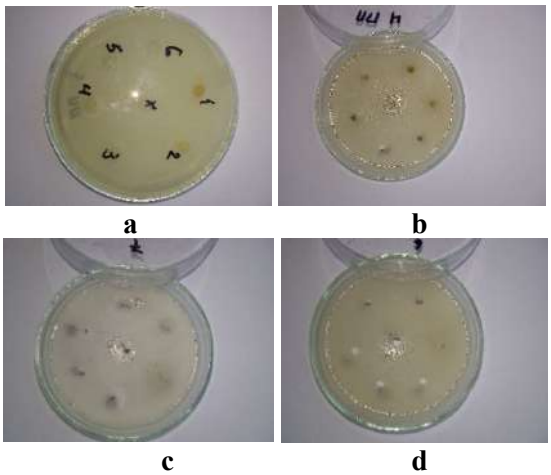

a **b** **c** **d**

Fig. 1. Bee Pollen – no zones of inhibition, dense bacterial growth*:* a) *Escherichia coli,* b) *Bacillus pumilus,* c) *Pseudomonas aeruginosa,* d) *Pseudomonas fluorescens*.

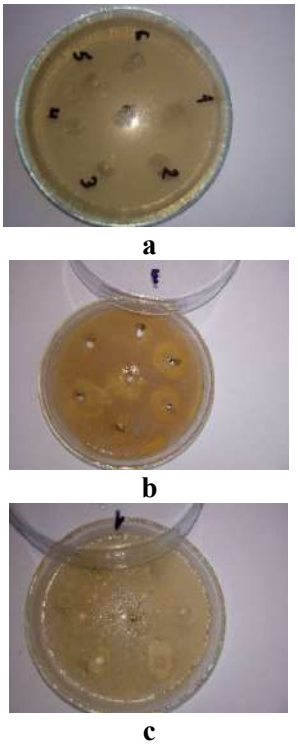

a **b** **c**

Fig. 2. Royal Jelly – no zones of inhibition, dense yeast growth: a) *Candida tropicalis*;

zones of inhibition observed with yeast growth: b) *Candida utilis*, c) *Saccharomyces cerevisiae*.

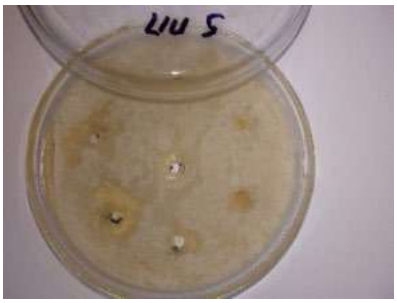

Fig. 3. Bee Pollen – zones of inhibition observed with yeast growth: *Trichosporon cutaneum*.

Our subsequent experiments were conducted using the same microorganisms, but in the presence of both preservatives, bee pollen and royal jelly, simultaneously in a 1:1 ratio, again in decreasing concentrations: 200, 100, 50, 25, 12.5, and 6.25, as shown in Tables 5 and 6.

From Table 5, it is evident that when bee pollen and royal jelly are combined, zones of inhibition appear at lower concentrations for most of the selected bacteria. In contrast, for yeasts, the opposite effect is observed: no zones of inhibition are seen at low concentrations for most of the selected yeasts.

Table 5. Zones of inhibition in bacteria in the presence of both bee pollen and royal jelly in a 1:1 ratio (mm)

Concentration, µl	B. subtilis	B. thuringiensis	Brevibacterium flavum	B. pumilus	E. coli	P. fluorescens	P. aeruginosa	Micrococcus spp.	Sarcina spp.	S. aureus
200	12	10	10	11	11	-	-	-	17	-
100	6	8	10	11	10	-	-	-	15	-
50	6	6	10	8	10	-	-	-	15	-
25	5	6	6	7	8	-	-	-	15	-
12.5	5	5	5	6	8	-	-	-	12	-
6.25	-	-	5	5	8	-	-	-	12	-
Control sample	-	-	-	-	-	-	-	-	-	-

Control sample – 95% ethanol

Table 6. Zones of inhibition in yeasts in the presence of both bee pollen and royal jelly in a 1:1 ratio (mm)

Concentration, µl	S. cerevisiae	C. tropicalis	C. utilis	R. rubra	T. cutaneum
200	12	-	20	-	16
100	10	-	16	-	-
50	10	-	-	-	-
25	8	-	-	-	-
12.5	6	-	-	-	-
6.25	6	-	-	-	-
Control sample	-	-	-	-	-

Control sample – 95% ethanol

a **b** **c**

Fig. 4. Bee pollen and royal jelly do not form sterile zones and lead to dense bacterial growth: a) *B. pumilus;* b) *B. thurigiensis;* c) *S. aureus.*

The experimental results show that bee pollen and royal jelly exhibit significant antimicrobial effects on the growth of microorganisms, with this effect varying depending on the type of microorganisms. (Fig. 4 and 5).

When combined, these natural products yield different outcomes based on the microorganism type.

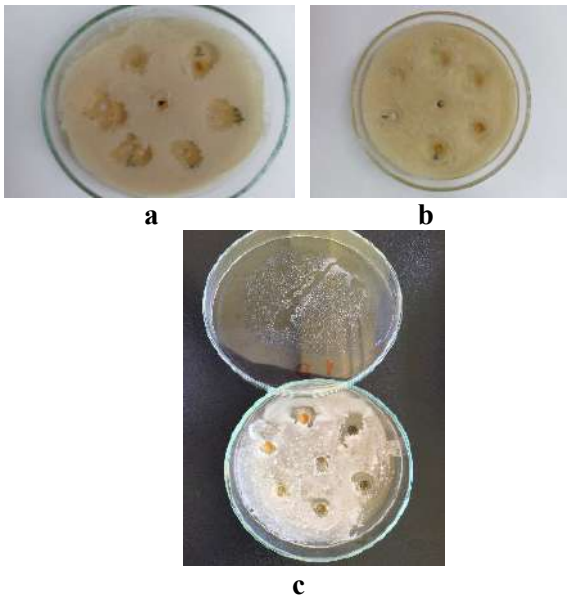

Fig. 5. Bee pollen and royal jelly form sterile zones in the presence of yeasts: a) *C. utilis*; b) *T. cutaneum;* c) *S. cerevisiae*.

CONCLUSIONS

The two natural products used in this study, bee pollen and royal jelly, exhibit inhibitory effects on the growth of selected bacteria and yeasts. Individually, bee pollen and royal jelly show stronger activity against yeasts, while their combination demonstrates enhanced antibacterial effects. Therefore, these natural products could potentially replace synthetic preservatives, particularly in the food and pharmaceutical industries.

REFERENCES

1. Kocot, J., Kiełczykowska, M., Luchowska-Kocot, D., et al. Antioxidant potential of propolis, bee pollen, and royal jelly: possible medical application. Oxid Med Cell Longev, 2018 (2018), 7074209, 2018.
2. Tutun, H., Kaya, M.M., Usluer, M.S., et al. Bee pollen: Its antioxidant activity. U Bee J; **21**, (2021), pp. 119-131.
3. Denisow, B., Denisow-Pietrzyk, M. Biological and therapeutic properties of bee pollen: a review. J Sci Food Agric, **96**, 13 (2016), pp. 4303-4309.
4. Mohdaly, A.A., Mahmoud, A.A., Roby, M.H., et al. Phenolic extract from propolis and bee pollen: composition, antioxidant and antibacterial activities. J Food Biochem., **39**, 5 (2015), pp. 538-547.
5. Sforcin, J.M., Bankova, V. Propolis: is there a potential for the development of new drugs? J Ethnopharmacol., **133**, 2 (2011), pp. 253-260.
6. Kasim, R. J. A study of antimicrobial activities of aqueous and ethanolic extract of bee pollen against, 2021. https://doi.org/10.21203/rs.3.rs-819311/v1
7. Al-Yousef, H.M., Amina, M., Alqahtani, A.S., Alqahtani, M.S., Malik, A., Hatshan, M.R., et al. Pollen Bee Aqueous Extract-Based Synthesis of Silver and Anti-Bacterial Activities. Pollen Bee Aqueous Extra Synth Silver Anti-Bacterial Act; pp. 1-12, 2020.
8. Metin, G. Effects of royal jelly and bee pollen on the growth of selected probiotic bacteria (bf. Animalis spp. Lactis, l. Acidophilus and l. Casei), J. Apic. Sci., **60** No. 2 (2016), pp 129-140.
9. FAO. Royal jelly, value added products from beekeeping, Chapter 6. Retrieved April 5, 2015, fromhttp://www.fao.org/docrep/w0076e/w0076e16. htm, 2013a.
10. Yatsunami, K. & Echigo, T. Antibacterial action of royal jelly. Bulletin of Faculty of Agriculture, **25**, 1 (1985), 13-22.
11. Bărnţiu, L. I., Mărghitaş, L. A., Dezmirean, D. S., Mihai, C. M., Bobiş, O. Chemical composition and antimicrobial activity of royal jelly – Review. Animal Science and Biotechnologies, **44**, 2 (2011), pp. 67-72.
12. Hatice, A. K., Hidayet, T., Muhammet, M. K., Melike, S. U., Soner, T., Ceren, Y., Sedat, S. and Erhan, K. Ethanolic extract of Turkish bee pollen and propolis: phenolic composition, antiradical, antiproliferative and antibacterial activities, Biotechnology & Biotechnological Equipment, **36**, 1 (2022), pp. 45-56.

ANNUAL OF ASSEN ZLATAROV UNIVERSITY, BURGAS
BULGARIA, 2024, v. LIII(1)

OBTAINING CALCIUM CARBONATE FROM EGGSHELLS BY LOW-TEMPERATURE PROCESSING

Ganka Kolchakova, Dimitrina Kiryakova
E-mail: gkolchakova@gmail.com

ABSTRACT

A new method was used to extract calcium carbonate ($CaCO_3$) from waste eggshells. It involved treating the eggshells with ethanol first and then heating them at 300°C. Ethanol is important for decomposing the organic material in the waste eggshells, making it easier to extract and purify $CaCO_3$. Using a low heating temperature helps maintain the quality of the extracted calcium carbonate and removes impurities effectively. Analyzing the extracted $CaCO_3$ using X-ray and FT-IR techniques was important to confirm the presence of calcite and ensure no other compounds were present. The microstructure was measured using a scanning electron microscope (SEM). This research demonstrates an effective and eco-friendly method that turns waste materials into valuable resources, promoting sustainable practices.

***Key words*:** waste eggshells, biomaterials, calcium carbonate, calcite, ethanol, calcinations

INTRODUCTION

By reusing eggshells, which are a significant waste product from the food industry, researchers have been able to extract calcium carbonate for a variety of industrial applications [1]. This not only reduces the amount of waste going to landfills but also provides a cost-effective and environmentally friendly alternative to sourcing calcium carbonate from traditional sources [2-3]. Given the abundance of eggshells produced globally, this innovative approach could have significant implications for the future of calcium carbonate production.

Calcium carbonate is one of the most common inorganic compounds [4-7]. Its versatility and widespread applications make it a valuable and essential mineral in many aspects of modern life. Potential uses of calcium carbonate derived from waste eggshells include use as a filler in various products such as paper, plastics, and rubber [8-9], as well as in the manufacture of paints and coatings [10]. It is also used as a filler in the production of cement [11-12] and concrete [13-14]. The high purity of calcium carbonate derived from eggshells makes it a desirable ingredient for pharmaceuticals and nutritional supplements [15-16]. In addition, its biodegradable nature makes it a suitable alternative for industries that want to reduce their impact on the environment but also reduce the need to extract and process natural calcium carbonate.

In many studies, researchers employed a chemical co-precipitation method to extract calcium carbonate from eggshell powder [17-18]. The process started by dissolving the eggshell in hydrochloric acid, followed by a reaction with sodium carbonate that precipitated the calcium carbonate. The resulting mixture was centrifuged to separate the solid precipitate from the supernatant, and the solid was washed with water to eliminate impurities. The final product was dried in an oven until a constant weight was achieved. Key challenges included ensuring complete dissolution of the eggshell, controlling the precipitation reaction for purity, and thorough drying to prevent decomposition. Successful extraction relied on appropriate equipment, chemicals, and careful monitoring throughout the procedure.

The aim of the present work is to examine a new method to extract calcium carbonate ($CaCO_3$) from waste eggshells. It involves treating the eggshells with ethanol first and then heating them at 300°C. The ethanol treatment helps to remove any impurities from the eggshells, allowing for a purer extraction of calcium carbonate. Heating the treated eggshells at 300 °C facilitates the breakdown of the organic compounds, leaving behind primarily calcium carbonate. This method offers a more efficient and environmentally friendly approach to utilizing waste eggshells for the production of calcium carbonate that can be used for various purposes.

EXPERIMENTAL

For the purposes of research and extraction of calcium carbonate from eggshells, it is necessary that they go through a series of pre-treatments to ensure the purity and quality of the final product.

Cleaning and drying of waste eggshells

The collected waste eggshells are washed with hot water without removing the membrane from them and left in the air for 24 hours. Then, they undergo further drying at 105°C until they reach a constant weight. Drying is critical to avoid agglomerates during subsequent steps.

Grinding and fractionation of waste eggshells

The dried eggshells were subjected to mechanical processing in a "Pulverisette 6" planetary ball mill. Fractionation of the obtained powders was carried out using a "Retsch AS 200" sieving machine. The aim was to reduce the particle size and increase the surface area for a better extraction of the calcium carbonate. A particle size fraction of 0.5 μm was selected for the purpose of the experiment.

Chemical and thermal treatment of eggshell powders

To remove surface organic contaminants, eggshell powders were mixed in a magnetic stirrer for 12 hours at 400 rpm and 25 °C with Sigma Aldrich's ethanol (C_2H_5OH, purity 96%). Following the treatment, we washed the powders with distilled water and filtered them. In order to completely remove organic impurities and increase the purity of extracted calcium carbonate without polymorphic conversion, the eggshell powders were heat treated at 300°C with a heating rate of 7°C/min for 1 hour in air environment.

Characterization

The resulting powders were subjected to various characterization methods. X-ray diffraction (XRD) was employed to identify the crystal structure of calcium carbonate, while Fourier-transform infrared spectroscopy (FTIR) was used to analyze the chemical composition. Scanning electron microscopy (SEM) was used to determine the morphology, particle size, and surface structure of the obtained samples.

XRD characterization was carried out on a Bruker 2D Phaser powder diffractometer. The samples were irradiated with CuKα radiation (λ = 1.54060 Å) and analyzed between 2-90° (2 theta).

Fourier transform infrared spectroscopy (FTIR) is a tool for identifying the types of chemical bonds in organic and inorganic molecules. The analysis was performed by using a Nicolet iS 50 FT-IR Thermo Scientific spectrophotometer in the interval 4000–400 cm^{-1}.

Scanning electron microscopy was performed on a JSM 6390 electron microscope (Japan) in conjunction with energy dispersive X-ray spectroscopy (EDS, Oxford INCA Energy 350) equipped with an ultrahigh resolution scanning system (ASID-3D) in regimes of secondary electron image and back scattered electron image.

RESULTS AND DISCUSSION

The phase composition of synthesized calcium carbonate ($CaCO_3$) was examined via X-ray diffraction (XRD) and is presented in Fig. 1. There were clear diffraction peaks in the 2θ range of 2° to 90° in the XRD pattern.

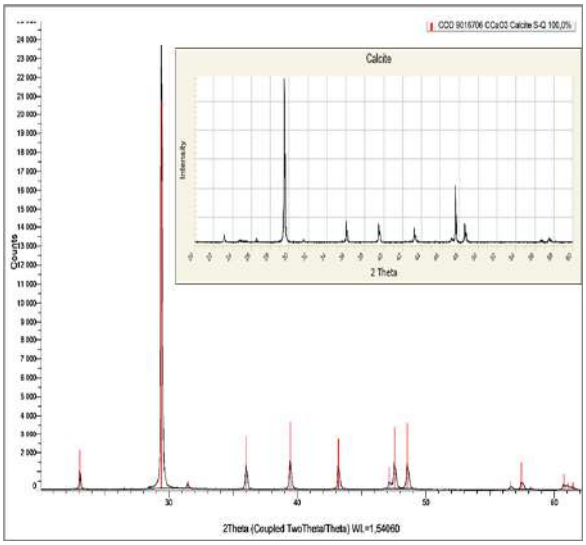

Fig. 1. XRD diffraction patterns of extracted $CaCO_3$

These peaks mostly matched the calcite phase of $CaCO_3$. Key peaks were identified at 2θ values of approximately 23.11°, 29.47°, 36.04°, 39.47°, 43.23°, 47.59°, 48.59°, and 57.48°, aligning with the Miller indices (012), (104), (110), (113), (202), (018), (116), and (122), indicative of the rhombohedral (hexagonal) structure of calcite [19-20].

These findings are consistent with reference data from the International Center for Diffraction Data (ICDD) [21]. Notably, the absence of significant peaks for other polymorphs such as aragonite and vaterite confirms the high purity of the calcite produced. In addition, the intensity of the

diffraction peaks showed a high degree of crystallization, with the peaks being narrow and distinct, indicating a well-crystallized calcite structure.

In order to confirm the chemical composition and the presence of calcite as the main form of calcium carbonate ($CaCO_3$), extracted from eggshells, Fourier transform infrared spectroscopy (FT-IR) was performed in the wavenumber range of 4000–400 cm^{-1}. The FT-IR spectrum presented in Fig. 2 showed characteristic absorption peaks corresponding to calcite. The strongest peaks were found between 1400 and 1500 cm^{-1} and 870 and 880 cm^{-1}. These ranges show the valence and deformation vibrations of the carbonate group (CO_3^{2-}) in $CaCO_3$ [22, 20].

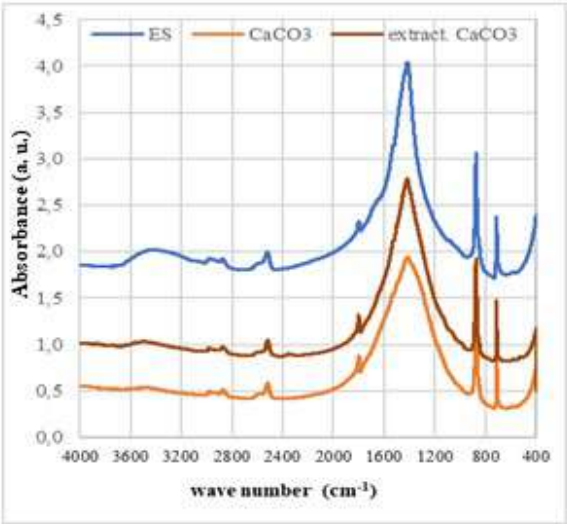

Fig. 2. FT-IR spectra of waste egg shells, extracted and commercial calcium carbonate.

The absence of peaks characteristic of aragonite (around 1080 and 700 cm^{-1}) and vaterite (at 1090 and 745 cm^{-1}) [23] further confirms that the studied material consists mainly of calcite.

In our previous work [20], the spectrum of waste eggshells revealed a complex structure. Along with the main peaks of calcium carbonate (Fig. 2), weaker ones are associated with organic substances in the matrix, such as those in the range 2900-3000 cm^{-1} (C-H stretching) and 3400–3500 cm^{-1} (O–H stretching) [23]. In contrast, the spectrum of the extracted calcium carbonate shows clear, well-defined peaks characteristic of the inorganic structure, with no significant organic bands.

The results of the performed XRD and FT-IR prove the efficiency of the used extraction method. Treatment with ethanol and subsequent temperature treatment completely removes organic impurities from eggshells. We identify the resulting calcium carbonate as pure calcite, devoid of any complex organic compounds from the original matrix.

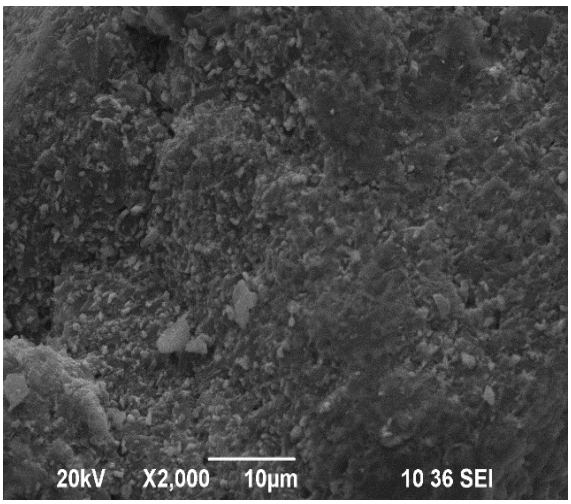

Fig. 3. SEM image of waste eggshells powders

The surface morphology of eggshell was observed from the SEM photographs. Fig. 3 clearly reveals the presence of irregularities and micrometer-sized pores in the shell structure. The surface appears rough as a result of the mechanical processing of the shells. We observe small agglomerates of accumulated particles. This could be attributed to a grinding treatment or a lack of particle separation. The presence of particles of different sizes is visible, ranging from small fragments to larger ones, all within the micron scale.

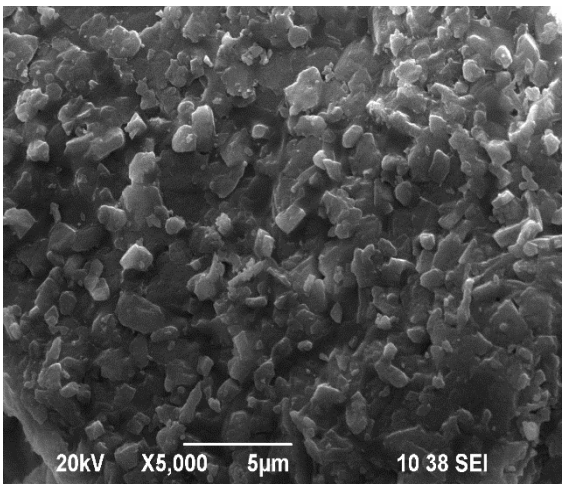

Fig. 4. SEM image of extracted $CaCO_3$

The SEM image in Fig. 4 presents $CaCO_3$ extracted from waste eggshells. At 5000x magnification, it reveals the distinct rhombohedral crystal structures characteristic of calcite. The crystals show well-defined edges and flat surfaces typical

of the morphology of this polymorph, with sizes ranging from 1 to 3 μm. The evenly distributed smaller crystals among the larger ones confirm the identification of the crystals as calcite, consistent with natural geological formations or slow crystallization processes under laboratory conditions [24].

CONCLUSION

The study demonstrates that a two-step process involving ethanol pretreatment and one hour of heating at 300°C can effectively convert eggshells into pure calcium carbonate. X-ray diffraction (XRD) analysis confirmed the formation of 100% calcite phase without impurities from other calcium carbonate polymorphs, such as aragonite or vaterite. Fourier transform infrared spectroscopy (FTIR) demonstrated the complete removal of organic residues. The presence of characteristic absorption bands associated with calcite indicates the successful transformation of eggshells. Additionally, scanning electron microscopy (SEM) revealed a homogeneous microstructure with well-defined crystalline surfaces characteristic of calcite. Overall, the findings highlight the efficiency of the proposed method for producing high-purity calcite from eggshells.

REFERENCES

1. Faridi, H. and A. Arabhosseini. Res. Agric. Eng., **64**, (2018), p. 104.
2. Waheed, M., M. Yousaf, A. Shehzad, M. Inam-Ur-Raheem, M. K. Khan, M. R. Khan, N. A. Abdullah, and R. M. Aadil. Trends Food Sci. Technol., **106**, (2020), p. 78.
3. Hart, A. J. Sustain. Circular Economy., **38**, (2020), p. 514.
4. Jimoh, O. A., K. S. Ariffin, H. B. Hussin and A. E. Temitope. Carbonates and Evaporites, **33**, (2017), p. 331.
5. Dizaj, S., Barzegar-Jalali, M., Zarrintan, M. H., Adibkia, K., & Lotfipour, F. Expert Opinion on Drug Delivery, 12(10), (2015), pp. 1649-1660.
6. Binks, B. P., K. Muijlwijk, H. Koman and A. T. Poortinga. Food Hydrocolloids, **63**, (2017), p. 585.
7. Galván-Ruiz, M., J. Hernández, L. Baños, J. Noriega-Montes and M. E. Rodríguez-García. J. Mater. Civil Eng., **21**, (2009), p. 694.
8. Owuamanam, S. and D. Cree. J. Compos. Sci., **4**, (2020), p. 70.
9. Roy, K., S. C. Debnath, N. Raengthon, and P. Potiyaraj. Polym. Eng. Sci., **59**, (2019), p. 1428.
10. Yoo, S., J. S. Hsieh, P. Zou and J. Kokoszka, Bioresour. Technol., **100**, (2009), p. 6416.
11. Grzeszczyk, S., T. Kupka, A. Kałamarz, A. Sudoł, K. Jurowski, N. Makieieva, K. Oleksowicz and R. Wrzalik. Constr. Build. Mater., **319**, (2022), p. 126006.
12. Nandhini, K. and J. Karthikeyan. Mater. Today Proc., **61**, (2022), p. 428.
13. Hamada, H. M., B. A. Tayeh, A. Al-Attar, F. M. Yahaya, K. Muthusamy and A. Humada J. Build. Eng., **32**, (2020), p. 101583.
14. Tan, Y. Y., S. I. Doh and S. C. Chin. Mag. Conc.Res., **70**, (2018), p. 662.
15. Rasheed, S. P., M. Shivashankar, S. Dev. and A. Azeem. Mater. Today Proc., **15**, (2019), p. 316.
16. Khan, S. R., S. Jamil, H. Rashid, S. Ali, S. A. Khan and M. R. S. A. Janjua, Chem. Phys. Lett., **732**, (2019), p. 136662.
17. Zhai, H., F. Liu, Y. Huang, Q. Yang, C. Tian and W. Zhou. Micropor. Mesopor. Mat., **329**, (2022), p. 111549.
18. Nawar, A., M. Ali, M. Mahmood, M. Anwar and Z. A. Khan. Mater. Today Commun., **24**, (2020), p. 101075.
19. Luo, X., X. Song, Y. Cao, L. Song and X. Bu. RSC Adv., **10**, (2020), p. 7976.
20. D. Kiryakova and G. Kolchakova, Annual of Assen Zlatarov University, **LI**, (2022), p. 21.
21. M. Sahadat Hossain and S. Ahmed. (2023). J. Saudi Chem. Soc., **27**, p. 101649.
22. Vagenas N.V., A. Gatsouli and C. G. Kontoyannis, Talanta, **59,** (2003), p. 831.
23. Kinaytűrk, N.K., B. Tunali and T. D. Altuğ, R. Soc. Open Sci., **8**, (2021), p. 210100.
24. Liendo, F., M. Arduino, F. A. Deorsola and S. Bensaid. Powder Technol., **398**, (2021), p. 117050.

ANNUAL OF ASSEN ZLATAROV UNIVERSITY, BURGAS
BULGARIA, 2024, v. LIII(1)

A CONCEPTUAL APPROACH TO THE DESIGN OF A SPECIALIZED MACHINE-BUILDING PLANT FOR THE REPAIR OF CYLINDER HEADS

Ivan Ivanov
E-mail: ivan_h_ivanov@mail.bg

ABSTRACT

In the study, the main tasks in the design of a specialized machine-building plant for the repair of cylinder heads are presented. Special attention is paid to the specifics of the repair activity: the construction of a number of different details and many technological options for processing, which also requires different approaches to the design compared to classical machine-building plants.

Key words: *cylinder head, repair, machine-building plant*

INTRODUCTION

The design of machine-building plants represents the solution of a number of complex tasks in the field of economy, technology and the organization of production. This solution involves many compromises due to limited resources [1-4]. Two conflicting concepts collide when designing a specialized cylinder head repair machine plant: on the one hand, the need to use specialized equipment and machinery, which is characteristic of mass engineering production, and on the other, the use of universal machines and typical technological processes, which is characteristic of repair work and single production. The collision of the two concepts for the design and construction of machine-building plants gives rise to a radically different approach to solving the main tasks – economic, technical, and organizational [5-8].

The purpose of the present study is to form a conceptual approach in the design and creation of a specialized machine-building plant for the repair of cylinder heads, taking into account the specifics of the activity.

RESULTS AND DISCUSSION

The diagnostics and repair of cylinder heads of internal combustion engines is a subject-specific activity aimed at achieving optimal reliability of the restored parts and assemblies through minimum costs of labour, time, materials, energy and consumables. When designing a machine-building plant, the first task to be solved is the economic one, which includes determining the production program, construction site, logistics of materials and energy sources, cooperation with other machine-building plants, preparation of a development plan, and so on.

Production program

The production program of a specialized machine-building plant for the repair of cylinder heads must be tailored to the needs of the auto repair groups developing their activities in the planned area of investment; the condition of the automobile fleet and the economic status of its owners; and the presence of other competing businesses.

Location of construction

The area and site of construction should be in areas intended for industrial activity or mixed ones – residential and industrial construction. An advantage when choosing the location for construction is the presence of a concentration of auto repair shops, because this reduces the time and cost of transporting cylinder heads for repairs and more.

Logistics of materials and energy sources

The repair of one-cylinder head requires many materials, tools, consumables and spare parts at the exact moment of their application in the necessary quantities. This requires stable and continuous supply chains. During the construction of the plant, it is necessary to connect it to the energy supply systems – electricity and heat, water supply and sewage, fuel gases for industrial purposes.

Cooperation with other plants

In repair production, cooperation between different plants is carried out in the technological process of restoration, using special welding and brazing methods, material technical assistance and know-how, but this is not mandatory.

Preparation of a development plan

The development plan should consider a detailed marketing study, the possibilities for the development of human resources – training, qualification, development of information management, and construction of a quality management system.

The technical tasks related to the design of a machine-building plant for the repair of cylinder heads are related to the design of the typical technological process for the restoration of cylinder heads, the selection of technological equipment and the number of machines and equipment, determining the number and qualifications of the personnel, solving the tasks of heating and cooling of work and auxiliary premises, ventilation, lighting, water supply and sewage. According to the type and quantity of the technological equipment, the production area is determined and the equipment plan is drawn up. Based on it, the transport links between the individual technological stations are built. The shape, dimensions and type of the building or buildings are determined, and measures for technical safety, fire and emergency safety, as well as environmental safety are prepared.

- The design of the typical technological process for cylinder head repair is the most important part of the plant design. Based on its results, the type of machines, fixtures and tooling for the repair production is determined.

- The type and number of technological equipment strongly depends not only on the typical technological process, but also on the financial and economic parameters of the investment process.

- The number and qualification of personnel is determined by the type and number of technological equipment. In repair production, the employment of highly qualified specialists working with different technological equipment is normally needed due to the specifics of the work which requires flexibility of the process.

- The creation of a suitable microclimate in the workplace is a prerequisite for increasing the quality of work and improving the health and safety of work conditions.

- Transport links in the plant are determined both by the arrangement of the technological equipment and by the technological path of restoration of each cylinder head. Because the activity is mainly carried out as a single or small serial production, the transport connections are not strictly regulated, and the section form of organization with a flow distribution of the sections turns out to be the most suitable arrangement.

- The shape, dimensions and type of the buildings must meet the relevant construction requirements, but also ensure maximum provision of natural light, heating and cooling, ventilation and fulfil all fire prevention requirements.

- Environmental safety from the point of view of the technical assurance of repair production is associated with the application of waste-free or low-waste technologies.

The third group of basic tasks that must be solved during the design of the plant are the organizational ones. These include the development of the management structure, the development of work organization and workplace issues, the specification of the order of acceptance of requests and customer service, the formation of technological and product traceability documents, the preparation and training of human resources and ensuring favourable working conditions.

- The management structure of a machine-building plant for the repair of cylinder heads is extremely simplified. This is related to the fact that the enterprise is micro or small according to the modern classification. For this reason, there are no departments, as in large engineering plants.

- The workplace, as a primary unit in production, has a direct impact on the quality of processed products. The main task in the design of the workplace is the creation of such an arrangement of the equipment where there are no completely unnecessary or irrational movements. Due to the multi-machine processing of the cylinder heads, the layout of the workplace must ensure minimal time loss during the transition from one working machine to another.

- The order of receiving requests and customer service is part of the company's quality management policy. In the repair production, each cylinder head is the object of single production and is a separate request, which implies an individual service approach.

- The production of technological documents and the traceability of the product when repairing cylinder heads are subject to the internal quality management system. Product traceability is facilitated by introducing an additional coding and classification system.

- The preparation and training of human resources in the specific activity of restoring cylinder heads is associated with training for work with the specific equipment, compliance with the technological and labour discipline, and compliance with the implemented quality management system.

- The construction of a specialized machine-building plant for the repair of cylinder heads is not an exception in terms of ensuring favourable and healthy working conditions. During its design and construction, provision should be made for sanitary and domestic premises, premises for recreation and rest, as well as facilities for them. Favourable working conditions motivate workers, and this is a prerequisite for higher quality.

CONCLUSIONS

In solving the three main groups of tasks – economic, technical and organizational, a specialized machine-building plant for the repair of cylinder heads is designed. Although economic tasks require cost reduction, this should not be at the expense of the quality of the repair work, the health and safety of the service personnel.

REFERENCES

1. Kozlov, V., I. L. Pichugova, Machine shops design: study aid. Tomsk, Tomsk Polytechnic University, TPU Publishing House, 2013, p.132
2. Suchkov A., V. Kostadinov, Design of machine-building plants. Ruse, State printing house “Danube”, 1990. p. 240.
3. Garcia-Diaz, A., Smith, J.M. Fundamental Principles of Facilities Planning and Design. In: Facilities Planning and Design. Springer, Cham., 2024, https://doi.org/10.1007/978-3-031-54259-6_1
4. Karpichev V., Sergeev K., Bolotina A. Modeling of Technological Processes of Machine-Building and Repair Manufacture. – Communications - Scientific letters of the University of Zilina, , **21**, 4 (2019), pp. 59-62.
5. Ivanov I., Organization, efficiency and cost of the technological process of restoration of cylinder heads from internal combustion engines, Industrial Technologies, **11**, 1 (2024), pp. 16-20.
6. Asef-Vaziri, L. Loop based facility planning and material handling. – European Journal of Operational Research, 2005, p. 1-11.
7. Boothroyd G., W.A. Knight, Fundamentals of Machining and Machine Tools. Second Edition. New York: MARCEL DEKKER, INC. 1989, p. 542
8. Minaeva U.V., Mathematical model of machine shops optimal design under a single machine chop criterion. – Vestnik VGTU, **10**, 1 (2012), p. 16-18.

ANNUAL OF ASSEN ZLATAROV UNIVERSITY, BURGAS
BULGARIA, 2024, v. LIII(1)

ON THE DAMAGE AND RESTORATION OF ENGINE EXHAUST MANIFOLDS

Ivan Ivanov
E-mail: ivan_h_ivanov@mail.bg

ABSTRACT

The study presents the causes of damage to exhaust manifolds. They are classified as mechanical and corrosion damage, and various technological options are presented to restore their operability, all of them including mechanical processing as part of a mandatory technological operation.

Key words: *exhaust manifolds, welding, grinding, corrosion, mechanical damage*

INTRODUCTION

Internal combustion engines are made up of many parts, the simultaneous faultless operation of which guarantees their reliability. Numerous studies have presented the results of damage to cylinder heads [1-5], valves [6, 7], and crankshafts [9] – the elements that are the basis of engine reliability. There are relatively few studies devoted to the damage and repair possibilities of exhaust manifolds [10-12].

The engine, as a thermodynamic system, converts the energy from fuel combustion from thermal to mechanical, and according to the first law of thermodynamics, the excess amount of energy is converted into another type – mechanical, thermal. One of the most important elements in any thermodynamic system is the cooler, which absorbs or removes excess heat. At a first glance, in internal combustion engines, the cooler is the cooling system in which a coolant (antifreeze) circulates. But its major purpose is to protect the parts involved in the construction of the engine, the cylinder block and cylinder head, from dangerously high temperatures. The main amount of heat is carried away by the hot gases through the exhaust system, which is the real cooler. The first contact of the exhaust gases is with the exhaust valves from the gas distribution mechanism; they pass through the exhaust channels of the cylinder head and reach the first structural detail of the exhaust system – the exhaust manifold. The purpose of the study is to identify and classify the main damages to the exhaust manifolds, as well as to present technological possibilities for their restoration.

RESULTS AND DISCUSSION

Exhaust manifolds are predominantly made of grey cast iron by casting or of stainless steel by welding. The choice of these alloys is due to the fact that cast iron and stainless steels can resist the high temperatures at which the collectors must operate. The exhaust manifolds are fixed to the cylinder head and the gasket to it. Cylinder heads are mainly made of aluminium alloys with significantly greater thermal expansion than cast iron and steel, which is a prerequisite for the occurrence of thermal stresses at the point of contact. The initial start of the engine is associated with an increase in the temperature of the parts that are directly involved in the combustion process: pistons, cylinders, cylinder head, valves. The exhaust gases pass through the collector at their maximum temperature even during the first operating cycle. While the pistons, cylinders, cylinder head and valves have a process of forced cooling and maintaining the temperature within normal working limits, the exhaust manifold is cooled solely by its contact with the surrounding air. During the entire process of engine operation, the collector is heated to high temperatures of 750°C [12], which makes it the most thermally stressed part of the engine. Of course, the heating process reaches a relatively equilibrium temperature during engine operation, and the cooling takes place after it is stopped. This cycle of heating and cooling the exhaust manifolds is repeated every time the engine is started and stopped, and during short stops, the manifold fails to cool completely and remains hot. As a result of this uneven thermal loading cycle, thermal stresses occur in the exhaust manifold that cause damage to both joining surfaces and raw func-

tional surfaces. The accumulation of thermal stresses in the material of the collector combined with the non-free variation of its dimensions near the cylinder head creates conditions for deformation of the joining surface or the appearance of cracks due to thermal fatigue. During long-term operation of a deformed exhaust manifold, the tensile stresses in the studs with which it is attached to the cylinder head increase, and when the limit values are reached, they are destroyed in a plane parallel to the connecting surface of the manifold.

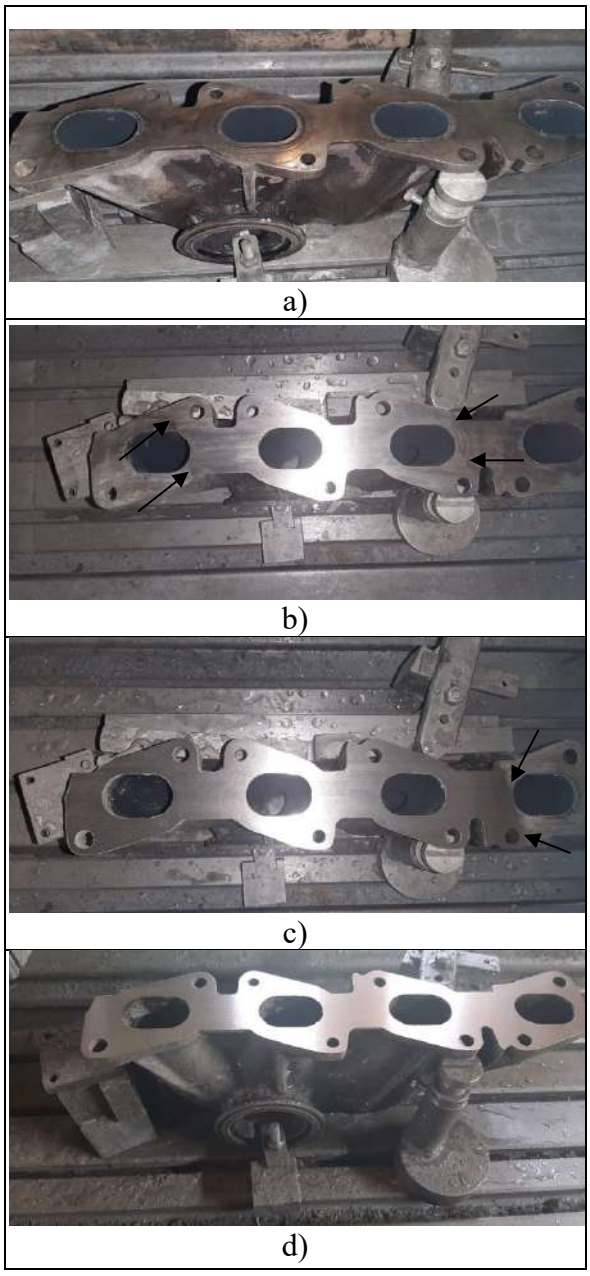

Fig. 1. Stages of exhaust manifold grinding: a) based on the table of a grinding machine; b) after removing a 0.4 mm layer of metal; c) after removing a 0.8 mm layer of metal; d) final grinding after removal of 1.07 mm layer of metal

As a result, the seal between the collector and the cylinder head is broken, the exhaust gases escape through this gap, and the lambda sensor gives wrong information about the state of the exhaust gases, which worsens both the power and environmental performance of the engine. The restoration of these collectors is carried out by mechanical processing of the deformed surface, removing a layer of metal until a flat surface is obtained. A technological option for recovery is shown in Fig. 1.

The exhaust manifold is based on supports placed on the table of a surface grinder. By successively removing a layer of metal, the surface is levelled and restored. Practice has shown that assembly of the collector to the cylinder head without mechanical processing until the surface is level is the cause of brittle destruction in the area of the fastening holes (Fig. 2).

Fig. 2. Exhaust manifold rebuilt by welding

In addition to thermal stress, exhaust manifolds are subject to intense corrosion. Gases that cause gas corrosion pass through the channels, and the outer walls are subjected to atmospheric corrosion during heating, cooling and the formation of condensation moisture on their surface. As a result of the intensity of corrosion, a significant reduction of the walls of the collectors is observed in some cases, mainly in the cast iron ones. In exhaust manifolds made of stainless steel, atmospheric corrosion is absent or very weak, and the most dangerous places are the surrounding areas of the welds, where the processes of initiation and development of cracks occur. In the case of cast iron collectors, the characteristic places for

the initiation and development of cracks are those parts of the casting in which there is a transition from thin to thick walls, local thinning, the places of connection of the pipes. These features also determine the difficulties in restoration by welding, and the choice of a method is particularly important, because cast iron is a material of poor weldability.

Fig. 2 and Fig. 3 show a stage of restoration by welding a cast iron exhaust manifold. The manual arc welding method with ENiFe electrodes was used. The initial limitation of the crack is carried out by drilling holes at its edges, forming a weld pool, which is filled with filler material. After welding is completed, the weld is deformed and the manifold is heat treated to reduce internal welding stresses. The final processing is mechanical – grinding the joining surface.

Fig. 3. Place of restoration by welding of an exhaust manifold made of cast iron

Based on many years of the author's observations, exhaust manifold failures can be classified as shown in Fig. 4:

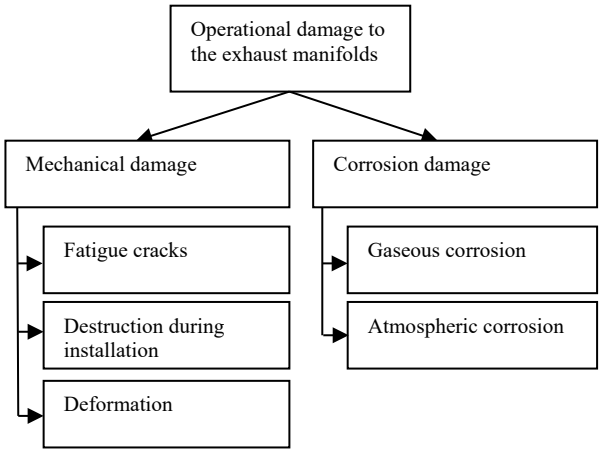

Fig. 4. Classification of damage to the exhaust manifolds

The occurrence of operational damage in the exhaust manifolds is a result of the simultaneous action of thermal and corrosion processes. For example, atmospheric and gas corrosion reduce the thickness of the collector wall and cause the appearance of a crack, the growth of which is favoured by thermal fatigue. As a result, the connecting surface to the cylinder head is also deformed.

CONCLUSIONS

From the observations regarding the operational damage of exhaust manifolds of internal combustion engines, it has been established that:

1. The appearance of operational damage in the exhaust manifolds is the result of a long-term operation, irrespective of the type of engine and fuel used.

2. The appearance of operational defects is always associated with deformation of the connection surface to the cylinder head, which determines its mechanical processing as the last technological operation to restore their working capacity.

3. The technology for restoring exhaust manifolds depends on the operational damage.

REFERENCES

1. Ivanov I., Kirov S., Uzuntonev T., Petrov P.; Characteristic defects of the basic components or parts of an IC engine during prolonged operational performance. AIP Conf. Proc., **2868**, 1, (2023); 020024.
2. Ivanov I., Rare damage to cylinder heads from internal combustion engines, Industrial Technologies, **11**, 1 (2024), p. 10-15.
3. Ivanov I. H., Destruction of a cast iron cylinder head in operation and after welding recovery, ACTA TECHNICA CORVINIENSIS – Bulletin of Engineering, **10**, 1 (2017), p.107-110.
4. Kirov S. K., Ivanov I. H., Structure and mechanical properties in welding of the grey cast iron details operated at high temperatures and pressure, Machine Building Techniques and Technology, **11**, (2006), p. 72-76.
5. Kirov S. K., Ivanov I. H. Typical defects in cylinder heads from different type of cars during the operation exploitation, Annual reports of Technical University – Varna, 2006, p.152-156.
6. Ivanov I., Operating failures of internal combustion engine valves, Transport, Ecology-Sustainable Development, Proceedings of the technical and scientific conference EKO Varna, 2017, p.75-78

7. Morehouse D., Porter J., Hiltz J., Brauss M. Diesel Engine Valve Failures. 56th Meeting of the Society for Machinery Failure Prevention Technology, At Virginia Beach, Virginia, USA, 2002
8. Raghuwanshi N., Pandey A., Mandloy R., Failure Analysis of Internal Combustion Engine Valves: A Review. International Journal of Innovative Research in Science, Engineering and Technology, **1**, 2 (2012), pp.173-181
9. Ivanov I.H., Destruction of Crankshafts from Internal Combustion Engines, Acta Technica Corviniensis – Bulletin of Engineering, **14**, 3 (2023), pp.81-84.
10. Mohammad A. S., Arash M., Mahdi R., Heydar A., Cracking failure analysis of an engine exhaust manifold at high temperatures based on critical fracture toughness and FE simulation approach, Engineering Fracture Mechanics, **211**, (2019), pp. 125-136
11. Chen G., Hu Y., Yan S., Zhu J., Yang L., Dong Z. Failure analysis of a natural gas engine exhaust manifold. Engineering Failure Analysis, **154** (2023), 107660.
12. Matteis P., Scavino G., Castello A., Firrao D., High Temperature Fatigue Properties of a Si-Mo Ductile Cast Iron. Procedia Materials Science, **3** (2014), pp. 2154-2159.

ANNUAL OF ASSEN ZLATAROV UNIVERSITY, BURGAS
BULGARIA, 2024, v. LIII(1)

TYPE 2 DIABETES AND THYROID DYSFUNCTION

Nikolay Kostadinov
E-mail: n.kostadinov_m.d@abv.bg

ABSTRACT

Type 2 diabetes has become a global pandemic with an increasing incidence. Dysfunction of the thyroid gland is an additional cardiovascular risk factor in patients with DM type-2. This has provoked our research interest in determining its frequency. The aim of the present analysis was to investigate the prevalence of thyroid dysfunction among patients with type-2 DM.

Key words: *Type 2 diabetes, thyroid dysfunction, frequency*

INTRODUCTION

Endocrine and metabolic diseases are among the most common modern chronic ailments. The prevalence and frequency of some of them have been well defined by the Bulgarian Society of Endocrinology in large population studies. In our country, the frequency of the most common endocrine diseases is as follows: diabetes mellitus (9.6%), increased fasting glycaemia (2.1%) and impaired glucose tolerance (1.6%), obesity (33.2%), metabolic syndrome (35.7%), osteoporosis (16.8%) and osteopenia (46.5%), hypovitaminosis D (75.6%), and thyroid pathology (10%) [1].

Diabetes mellitus (DM) is a group of metabolic diseases characterized by hyperglycaemia resulting from defects in insulin secretion, insulin action, or both [2]. The prevalence of type-2 DM is expected to increase in the future due to unhealthy lifestyles and an increasingly aging population [3].

Thyroid hormone deficiency and low circulating thyroid hormone levels, even within the normal reference range, may be associated with an increased risk of developing type-2 DM, particularly in prediabetic population. The prevalence of overt and subclinical hypothyroidism is higher in patients with type-2 diabetes compared to the general population. In prospective studies, it has been shown that not only hypothyroidism, but also changes in the serum level of TSH and/or thyroid hormones within reference limits are associated with the risk of developing type-2 diabetes. A study conducted in Rotterdam examined the relationship between thyroid function, incidence of type-2 DM, and progression from prediabetes to diabetes in participants without diabetes at baseline. At a mean follow-up of 7.9 years, higher TSH levels and lower fT4 levels were associated with an increased risk of diabetes and a progression from prediabetes to diabetes [4].

These are the most common forms of thyroid dysfunction in patients with type-2 diabetes mellitus, with a prevalence of between 6-20% in different ethnic groups. Female gender, advanced age, obesity, a positive anti-TPO test, and hospitalization are factors associated with an increased risk of developing hypothyroidism in type-2 DM. An increased risk of progression from subclinical to overt disease has been reported in adults with type-2 DM. The rate of progression was 5% per year in patients with type-2 DM positive for anti-TPO. Regarding hyperthyroidism, there is a significant and unknown correlation between advanced age and the presence of goiter and the occurrence of hyperthyroidism in the diabetic population, indicating that toxic polynodosis goiter is a more common cause of hyperthyroidism than Based disease [3].

The need for screening programs in patients with thyroid dysfunction and diabetes mellitus is a controversial issue. Data are currently insufficient to evaluate specific screening tests (only TSH, TSH and anti-TPO, TSH and fT4), frequency of screening and, accordingly, cost-benefits. In patients with type-2 diabetes mellitus, screening is recommended because the onset of thyroid dysfunction may further increase the long-term morbidity and mortality associated with type-2 diabetes mellitus [5].

MATERIAL AND METHODS

The aim of the present analysis was to investigate the prevalence of thyroid dysfunction among patients with type-2 DM without previously diagnosed thyroid disease.

The distribution of patients is shown in Table 1. 37 patients were randomly examined, respectively 11 men with a relative share of 29.7% and 26 women with a relative share of 70.3%. All of them had type 1 diabetes. The research period was August - September 2024. All patients were tested for TSH, fT4, and anti-TPO.

Table 1 Distribution of patients by gender

Gender	Number	(%)
male	11	29.7
female	26	70.3
Total	37	100.0

The average age of the patients was 65.51 (±9.91 SD) and is reflected in Table 2.

Table 2 Average age of patients

Statistics		
Age		
N	Valid	37
	Missing	0
Mean		65.51
Std. Deviation		9.912
Minimum		48
Maximum		80

RESULTS

In the studied group, it was found that 11% (n-4) had a reduced function of the thyroid gland, hypothyroidism in three patients, and subclinical hypothyroidism in one patient. The data from this study confirmed the prevalence of thyroid dysfunction in patients with DM type-2 in the Burgas region, which is in accordance with the currently known world data.

CONCLUSIONS

Thyroid dysfunction is a common disorder in patients with type-2 diabetes mellitus. The occurrence of thyroid disease can worsen the prognosis of diabetes. It would be good to consider periodic screening for thyroid dysfunction in patients with type-2 diabetes and vice versa. Unrecognized and untreated thyroid dysfunction can negatively affect the underlying diabetes and its complications. Patients with DM and thyroid dysfunction are not only physically sick, but also have an increased risk of complications of the disease.

REFERENCES

1. Borisova, A-M., Epidemiology of endocrine diseases in Bulgaria, Bulgarian Society of Endocrinology, 2016.
2. Craig M.E., Hattersley A., Donaghue KC. Definition, epidemiology and classification of diabetes in children and adolescents. Pediatric diabetes, **10**, 12 (2009), pp. 3-12.
3. Biondi, B.,Kahaly, G.J., Robertson, R.P. Thyroid dysfunction and diabetes mellitus: two closely associated disorders, Endocr Rev., **40**, 3 (2019), pp. 789-824.
4. Chaker, L., Ligthart, S., Korevaar, T.I., Hofman, A., Franco, O.H., Peeters, R.P., Dehghan, A. Thyroid function and risk of type 2 diabetes: a population based prospective cohort study. BMC Med. 30, **14**, 1: (2016), p. 150.
5. Karla S., Aggarwal S., Khandelwl D., Thyroid dysfunction and type 2 diabetes mellitus: screening strategies and implications for management. Diabetes Ther., **10**, 6 (2019), pp. 2035-2044.

ANNUAL OF ASSEN ZLATAROV UNIVERSITY, BURGAS
BULGARIA, 2024, v. LIII(1)

MONITORING GAMMA RADIATION BACKGROUND AND SURFACE CONTAMINATION OF LAND AND SAND

Sabina Nedkova, Plamena Atanasova, Kaloyan Ivanov
E-mail: sabina_nedkova@abv.bg

ABSTRACT

Ionizing radiation forms a substantial part of the environment in which the organisms live. Depending on its sources, it has a natural or technological origin, which affects their life and development. The following analysis is based on the results of radiological monitoring of gamma radiation background and ambient dose equivalent rate and a monitoring of a surface contamination of soil and sand measured with a personal portable dose rate meter in two monitoring locations in terrestrial and marine environment systems.

Key words: *ionizing radiation, gamma background, surface contamination*

INTRODUCTION

Ionizing radiation has been part of the environment since the Earth was formed as a solid planet, more than 4.5 billion years ago. Depending on its origin, ionizing radiation forms a natural radiation background, when it comes from natural ionizing sources, most of which are found in soil, rocks and sands (natural radioactive elements of the Uranium-Thorium series), cosmic radiation, radon gas, etc.; and artificial radiation background, from sources of human activity related to nuclear energy and its use for peaceful and military purposes, medical diagnosis and treatment, etc. Because of its ability to change the matter through which it passes and its high energy, ionizing radiation is very dangerous for living organisms and forms the so-called Radiation risk. In its impact on living organisms, two features of this risk are important: the absence of any sensation at the moment of irradiation, since there are no receptors for this type of energy in living organisms, and the large discrepancy between the absorbed energy and the radiobiological effect (a small dose of ionizing radiation can cause a large effect).

Sources and routes of entry of radionuclides into the external environment

Radioactive substances can enter the biosphere as a result of testing nuclear devices in various natural environments, or in the form of radioactive waste from industrial, power reactors, or from uncontrolled emissions of radionuclides into the external environment as a result of accidents in a nuclear environment. A limited amount of radioactive materials enters the environment as a result of the extraction of uranium ore, the processing of separated fuel elements in order to obtain ^{239}Pu - nuclear fuel, as well as a result of the transportation and storage of radioactive production waste. Uranium ore contains no more than 0.2% uranium, as well as radionuclides such as ^{226}Ra, ^{210}Pb, ^{210}Po. As a result, in the area of uranium mining and enrichment, the background of natural radioactivity increases [1].

Physicochemical state of radionuclides in water and soil

The evaluation of the possibilities to reduce the content of radionuclides in environmental objects necessitates the need to know their condition and form in these objects. For example, nearly 73.7% of the total amount of ^{90}Sr released in the environment is almost entirely in water-soluble form, and the amount of ^{137}Cs is 44.9%. The mobility of ^{90}Sr deposits in soil is also quite high: about 60% of ^{90}Sr is found in exchangeable form. In soil, radionuclides are in different physical and chemical states and, since their accumulation by plants is determined by their relative bioavailability and change over time, it is necessary to have data on the status and forms of radionuclides in soil. The amount of water-soluble ^{89}Sr is the greatest in soil with low pH and minimal content of exchangeable Ca^{+2}. Almost all radioactive strontium in the soil is in a mobile form, while the bulk of the caesium is sorbed to the soil quite strongly, and only 1% of it can pass into the aqueous extract and less than a third into the ammonium acetate solution [1].

EXPERIMENT

The subject of the present research is radiological monitoring, which was developed as:

- monitoring of gamma radiation background and ambient dose equivalent rate;
- monitoring of surface contamination of soil and sand in two monitoring locations in terrestrial and marine environmental systems;

Fig. 1. Portable doze rate meter and Alpha/Beta/Gamma external 15 cm^2 CSP probe w/pancake G-M.

The monitoring locations for gamma radiation background and surface contamination were selected to represent two ecosystems: a terrestrial (monitoring point No. 1 in Prof. Dr Assen Zlatarov University campus) and a marine (two monitoring points No. 2 and No. 3 on Burgas beach) environmental system in the town of Burgas, Bulgaria. The collected data include gamma radiation background/air doze rates registered at the three monitoring points and surface contamination of dry and wet sand in the monitoring location on the beach and on land in the monitoring location in the university for a period of nine months (from January to September 2024). The gamma radiation background was measured as H*(10), ambient dose equivalent rate in µSv/h with a personal portable dose rate and survey meter Radiagem 2000 (Fig. 1). *H*(10) reflects the absorption of gamma radiation in a tissue-equivalent area (equivalent to the human body), i.e. through H*(10), the human absorbed dose can be directly calculated.*

The monitoring of surface contamination or the presence of a radioactive substance on a land and sand surface (in the two monitoring locations), was measured with an Alpha/Beta/Gamma external 15 cm^2 CSP probe w/pancake G-M NOM 0006364 SABG-15+, as seen in Fig.1. *Contamination shall mean the presence of a radioactive substance on a surface in quantities in excess of 0.4 Bq/cm² for beta and gamma emitters and low toxicity alpha emitters, or 0.04 Bq/cm² for all other alpha emitters* [2].

RESULTS

Gamma Radiation background, Surface contamination of dry sand and wet sand

The correlation analysis shows a positive correlation amongst the three data types: the gamma radiation background, the surface contamination of wet (closest to the sea) and dry sand, as shown in Table 1.

Table 1. Correlation of Gamma radiation, Surface contamination of wet and dry sand (Monitoring points No. 2 and No. 3)

Correlations

		Gamma Radiation sand µSv/h	Surface Contamination Dry Sand [Bq/cm2]	Surface Contamination Wet Sand [Bq/cm2]
Gamma Radiation sand µSv/h	Pearson Correlation	1	,362	,884**
	Sig. (2-tailed)		,339	,002
	N	9	9	9
Surface Contamination Dry Sand [Bq/cm2]	Pearson Correlation	,362	1	,480
	Sig. (2-tailed)	,339		,191
	N	9	9	9
Surface Contamination Wet Sand [Bq/cm2]	Pearson Correlation	,884**	,480	1
	Sig. (2-tailed)	,002	,191	
	N	9	9	9

The overall relation of the analyzed variables is positive with higher statistical significance in the relation Gamma Radiation background on the beach and Surface contamination of wet sand. The results are also presented in their aspect of positive correlation in the scatter diagram in Fig. 2, of the same data relation, with the results for each of the months of collecting data, using the number of the month as a describing number of the point (January, presented as point 1; February, presented as point 2, etc.). In this way, the nine points in the diagram describe the nine months of data collection.

Gamma Radiation background, Surface contamination of land

The correlation analysis shows a positive correlation among the two data types: the gamma radiation background and the surface contamination of soil, as shown in Table 2. The overall relation of the analyzed variables is positive with higher statistical significance in the relation Gamma Radiation background on the land area (monitoring point No. 1 in the campus of the University) and

Surface contamination of the soil at the same monitoring point.

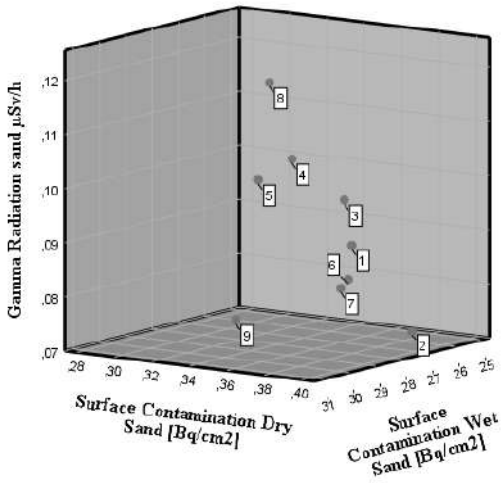

Fig. 2. Simple 3-D Scatter of gamma radiation sand, by surface contamination dry sand, by surface contamination wet sand

Table 2. Correlation of Gamma radiation, Surface contamination of soil (Monitoring point No.1)

Correlations

		Gamma Radiation University µSv/h	Surface Contamination Soil [Bq /cm2]
Gamma Radiation University µSv/h	Pearson Correlation	1	,442
	Sig. (2-tailed)		,233
	N	9	9
Surface Contamination Soil [Bq /cm2]	Pearson Correlation	,442	1
	Sig. (2-tailed)	,233	
	N	9	9

The gathered data is also presented as a graphic, with the results for each of the months of collecting data, using the number of the month as a describing number on the horizontal line of the diagram, (January is month 1, February is month 2, etc.) in Fig. 3.

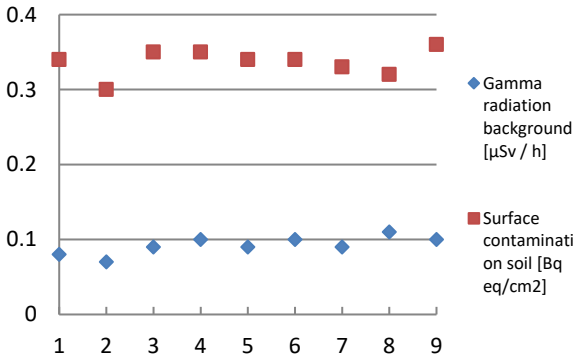

Fig. 3. Relation between the gamma radiation background and the surface contamination of soil at monitoring point No. 1, in the University campus.

It is seen that the values of the gamma radiation and the surface contamination are related, with similar distribution of the data (the increase of the values of gamma radiation in most of the cases means increase of the values of the surface contamination, which proves the positive correlation of the parameters).

Gamma radiation background on the beach and at the University

The assessed data on the gamma radiation at monitoring points No. 1 and No. 2 and 3 are within the limits of the so called "natural gamma background" of 0.06-0.40 µSv/h. The descriptive analysis in Table 3 shows mean values of 0.09 µSv/h.

Table 3. Descriptive analysis of Gamma radiation on the beach and at the University

	N	Minimum	Maximum	Mean	Std. Deviation
Gamma Radiation sand µSv/h	9	,07	,12	,0911	,01764
Gamma Radiation University µSv/h	9	,07	,11	,0922	,01202
Valid N (listwise)	9				

The descriptively assessed data on surface contamination of the soil detected (monitoring point No. 1) and of dry and wet sand (monitoring points No. 2 and 3) is lower than the limit of alpha type contamination, 0.4 [Bq/cm^2], and beta type contamination, 4 [Bq/cm^2], with mean values of 0.36, 0.28 and 0.34 [Bq eq/cm^2], as listed in Table 4. It can be seen that the highest values of surface contamination were detected on dry sand, which can be explained with the low humidity of the sand surface, smaller sand particle sizes in comparison to soil particles and the highest moisture content in the soil as well as the relation between the dustiness and the surface contamination.

Table 4. Descriptive analysis of Surface contamination detected on soil and dry and wet sand

	N	Minimum	Maximum	Mean	Std. Deviation
Surface Contamination Dry Sand [Bq/cm2]	9	,29	,39	,3567	,03202
Surface Contamination Wet Sand [Bq/cm2]	9	,25	,31	,2767	,01871
Surface Contamination Soil [Bq /cm2]	9	,30	,36	,3367	,01803
Valid N (listwise)	9				

CONCLUSION

The analysis of the data from the radiological monitoring carried out on the two monitoring lo-

cations in marine and terrestrial ecosystems (marine location: dry and wet sand monitoring points, and terrestrial location: land point) as:

- monitoring of gamma radiation background and ambient dose equivalent rate, measured in μSv/h;
- surface contamination of wet and dry sand and soil, measured in Bq eq /cm^2;

The following results were obtained:

- The correlation analysis shows a positive correlation amongst the three data types: gamma radiation background, surface contamination of wet and dry sand, as shown in Table 1. The overall relation of the analyzed variables is positive with higher statistical significance in the relation Gamma Radiation background on the beach and Surface contamination of wet sand.
- The gamma radiation background, measured as H*(10), ambient dose equivalent rate in μSv/h, on the sand and the land is within the safe limits of 0.06 to 0.40 [μSv/h].
- The surface contamination detected on wet and dry sand and soil is lower than the limit of alpha type of contamination and could be considered safe.

ACKNOWLEDGMENT

This work was supported by NIS 479/2023 Scientific Research Sector programme of Prof. Dr. Asen Zlatarov University, Burgas.

REFERENCES

1. Bajenov V.A., at al, Vrednje himicheskie veshtestva, Radiosktivnie veshtestva, Leningrad, Chemistry, 1990.
2. Regulations for the Safe Transport of Radioactive Material, 2018 Edition, Specific Safety Requirements No. SSR-6 (Rev. 1).

ANNUAL OF ASSEN ZLATAROV UNIVERSITY, BURGAS
BULGARIA, 2024, v. LIII(1)

MULTIPLE LINEAR REGRESSION ANALYSIS ON MENTAL HEALTH DISORDERS IN BULGARIA

Stanislav Popov
E-mail: stani_popov@yahoo.com

ABSTRACT

Mental illness, also called mental health disorders, refers to a wide range of mental health conditions or disorders that affect people's mood, thinking and behaviour. Mental health conditions include mental disorders and psychosocial disabilities as well as other mental states associated with significant distress, impairment in functioning, or risk of self-harm. The present paper focuses on finding dependencies between the most common types of mental disorders among the population of Bulgaria. Multiple linear regression is performed over the collected data for the period 1990-2022. The aim is to facilitate the decision that more efforts should be concentrated in coping with the most correlated types of mental disorders.

Key words: *mental health, machine learning, multiple linear regression*

INTRODUCTION

Mental health is an integral part of health and well-being, as reflected in the definition of health in the Constitution of the World Health Organization: "Health is a state of complete physical, mental and social well-being and not merely the absence of disease or infirmity." Mental health, like other aspects of health, can be affected by a range of socioeconomic factors that need to be addressed through comprehensive strategies for promotion, prevention, treatment and recovery in a whole-of-government approach [1, 2].

The term "mental disorders" used in this paper denotes a range of mental and behavioural disorders that fall within the International Statistical Classification of Diseases and Related Health Problems, Tenth revision (ICD-10) [3]. These include disorders that cause a high burden of disease such as depression, bipolar affective disorder, schizophrenia, anxiety disorders, dementia, substance use disorders, and intellectual disabilities.

The most widely spread mental disorders are schizophrenia, anxiety, depression and eating disorders as depression alone accounts for 4.3% of the global burden of disease [4, 5]. As such, they are the focus of analysis in the present research.

MENTAL HEALTH DATA

Data on mental health are crucial for monitoring mental health and its evolution over time and locations, developing effective policies and addressing the growing mental health challenges. They are collected at national, EU and international levels. At EU level, Eurostat issues online publications on public health, provides data on many aspects of public health and self-reported data from the European Health Interview Survey (EHIS), which can be found in [6, 7].

There are notable variations in mental health across EU countries (see Fig. 1) [8]. Factors such as socio-economic conditions, access to healthcare and cultural attitudes towards mental health contribute to these disparities. Data from Eurofound's e-survey indicate that in the spring of 2022, more than one in two people (55%) could be considered at risk of depression on average across EU countries [9].

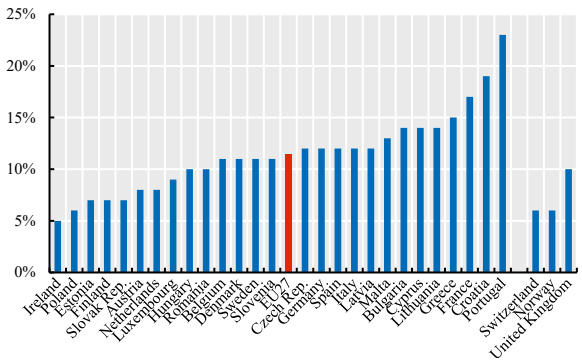

Fig. 1 Share of population with mental disorders in EU and EEA

According to The Mental Health Atlas [10] published by The World Health Organization and The National Statistical Institute of Republic of Bulgaria (Health Section), a dataset is created, which consists of the types of mental disorders (Anxiety, Eating disorders and Depression) as a share of population in Bulgaria (Fig. 2).

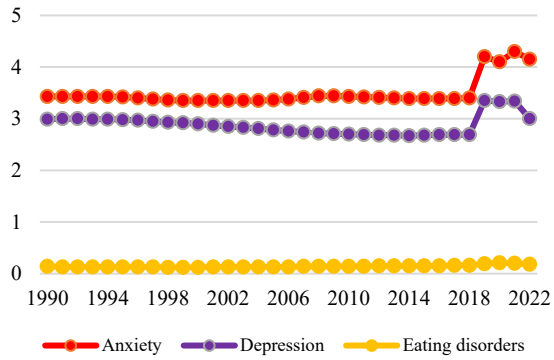

Fig. 2. Mental disorders prevalence in Bulgaria (1990 - 2022)

REGRESSION ANALYSIS: DEFINITION

Regression analysis is a set of statistical methods used for the estimation of relationships between a dependent variable and one or more independent variables. It can be applied to assess the strength of the relationship between variables and for modelling the future relationship between them.

Regression analysis includes several variations, such as linear, multiple linear, and nonlinear (Fig. 3). The most common models are simple linear and multiple linear. Nonlinear regression analysis is commonly used for more complicated data sets in which the dependent and independent variables show a nonlinear relationship.

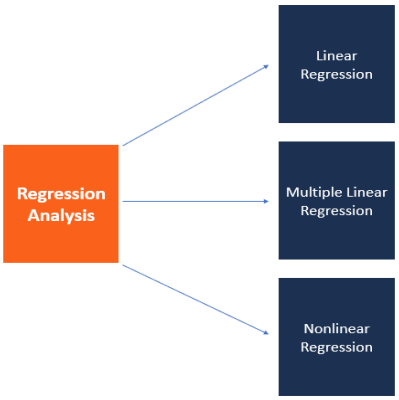

Fig. 3 Types of regression analysis

Simple linear regression is a model that assesses the relationship between a dependent variable and an independent variable. The simple linear model is expressed using the following equation:

$$Y = a + bX + \epsilon$$

Where:

- Y – Dependent variable
- X – Independent (explanatory) variable
- a – Intercept
- b – Slope
- ϵ – Residual (error)

Multiple linear regression analysis is essentially similar to the simple linear model, with the exception that multiple independent variables are used in the model. The mathematical representation of multiple linear regression is:

$$Y = a + bX_1 + cX_2 + dX_3 + \epsilon$$

Where:

- Y – Dependent variable
- X_1, X_2, X_3 – Independent (explanatory) variables
- a – Intercept
- b, c, d – Slopes
- ϵ – Residual (error)

Multiple linear regression follows the same conditions as the simple linear model.

RESULTS

The three types of mental disorders are Depression, Anxiety and Eating disorders. Firstly, linear regression is performed over the collected data for the 2019-2022 period in Bulgaria. The dependable variable is Eating disorders. Fig. 4 and Fig. 5 show the results from the analysis for Anxiety and Depression, respectively.

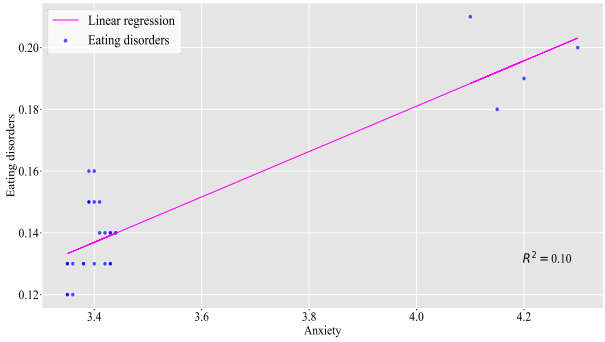

Fig. 4 Anxiety – Eating disorders

Both R-squared values are low: 0.10, which indicates that the model cannot be determined as reliable. Thus, a multiple linear regression is performed to further improve the model.

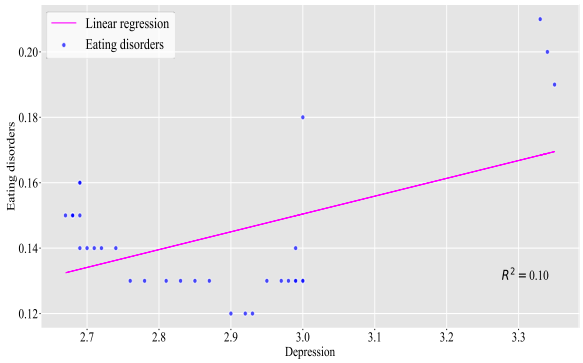

Fig. 5 Depression – Eating disorders

Fig. 6 and Fig. 7 represent the result, while a fragment of the programing code is presented below:

```
#Prepare the data
X = df[['Anxiety', Depression']].values.reshape(-1,2)
Y = df['Eating disorders']

#Train the model
ols = linear_model.LinearRegression()
model = ols.fit(X, Y)
predicted = model.predict(model_viz)

#Evaluate
r2= model.score(X, Y)
#Plot
fig = plt.figure(figsize=(12, 4))
ax1 = fig.add_subplot(131, projection='3d')
ax2 = fig.add_subplot(132, projection='3d')
ax3 = fig.add_subplot(133, projection='3d')
for ax in axes:
    ax.plot(x, y, z, color='k', zorder=15, linestyle='none', marker='o', alpha=0.5)
    ax.scatter(xx_pred.flatten(), yy_pred.flatten(), predicted, facecolor=(0,0,0,0), s=20, edgecolor='#70b3f0')
    ax.set_xlabel('Porosity (%)', fontsize=12)
    ax.set_ylabel('Brittleness', fontsize=12)
    ax.set_zlabel('Gas Prod. (Mcf/day)', fontsize=12)
    ax.locator_params(nbins=4, axis='x')
    ax.locator_params(nbins=5, axis='x')
…
```

The *R*-squared value from the multiple linear regression rises to 0.46, which indicates a significant improvement compared to the previous results.

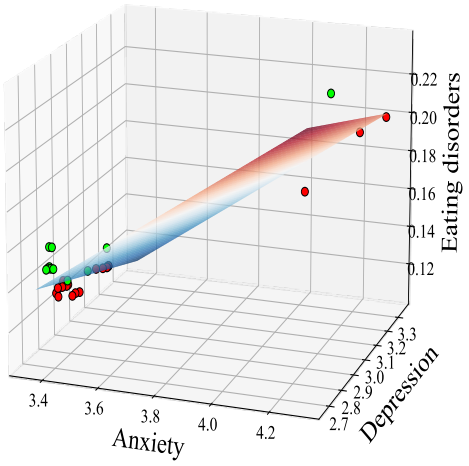

Fig. 6. Multiple linear regression, view 1

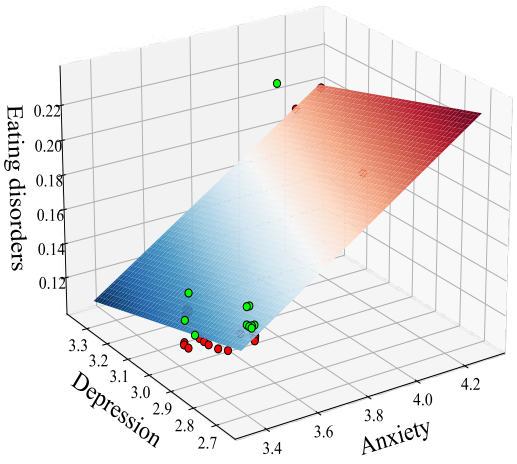

Fig. 7. Multiple linear regression, view 2

CONCLUSION

This paper examines the dependencies between the most common types of mental disorders (Depression, Eating disorders and Anxiety) in Bulgaria for the 1990-2022 period. Firstly, linear regression analysis was performed to calculate *R*-squared values for the Anxiety-Eating disorders and Depression-Eating disorders pairs. The results show little relationship between the pairs. Then, multiple regression was fitted into the model so that better *R*-statistics values could be obtained. Adding the second predictor improved the model significantly.

REFERENCES

1. Ahmedani, BK.: Mental health stigma: society, individuals, and the profession, Journal of social work values and ethics, **8**, 2 (2011), pp. 4-16.

2. Knapp, M., Wong, G.: Economics and mental health: the current scenario. World Psychiatry, **19**, 1 (2020), pp. 3-14.
3. International Classification of Diseases, Tenth Revision, Clinical Modification, April 2024, https://www.cdc.gov/nchs/icd/Comprehensive-Listing-of-ICD-10-CM-Files.htm
4. Sickel, A. E., Seacat, J. D. and Nabors, N. A.: Mental health stigma update: A review of consequences. Advances in Mental Health, **12**, 3 (2014), pp. 202-215.
5. Dementia: a public health priority. Geneva: World Health Organization; 2012, https://apps.who.int/iris/handle/10665/75263.
6. Eurostat, Statistical reports, https://ec.europa.eu/eurostat/web/main/publications/statistical-reports.
7. Publication Office of European Union, https://op.europa.eu/en/publication-detail/-/publication/78325641-8fa2-11ea-812f-01aa75ed71a1.
8. Health at a Glance: Europe 2022: State of Health in the EU Cycle, OECD iLibrary, https://www.oecd-library.org/sites/507433b0-en/1/3/2/1/7/index.html?itemId=/content/publication/507433b0-en&_csp_=69a1197833db420974a2940c01518500&item-IGO=oecd&itemContentType=book#
9. Eurostat news article, "7.2% of people in the EU suffer from chronic depression", https://ec.europa.eu/eurostat/web/products-eurostat-news/-/edn-20210910-1.
10. Mental Health Atlas, WHO, Geneva, Switzerland, https://iris.who.int/bitstream/ handle/10665/345946/9789240036703-eng.pdf?sequence=1.

ANNUAL OF ASSEN ZLATAROV UNIVERSITY, BURGAS
BULGARIA, 2024, v. LIII(1)

GENERALIZED NET MODEL OF EXPECTATION-MAXIMIZATION ALGORITHM

Stanislav Popov
E-mail: stani_popov@yahoo.com

ABSTRACT

The Expectation-Maximization (EM) algorithm is a way to find maximum-likelihood estimates for model parameters when your data is incomplete, has missing data points, or has unobserved (hidden) latent variables. The algorithm process is presented in this research with the usage of Generalized nets. The constructed Generalized net can be used for describing and monitoring the parallel processes in the EM algorithm.

Key words: *Generalized nets, machine learning, EM-algorithm*

INTRODUCTION

Expectation–Maximization is successfully applied in data mining as an iterative method that attempts to find the maximum likelihood estimator of a parameter θ of a parametric probability distribution. To use EM, we are given some observed data y, a parametric density $p(y|\theta)$, a description of some complete data x that we wish we had, and the parametric density $p(x|\theta)$. We assume that the complete data can be modelled as a continuous random vector X with density $p(x|\theta)$, where $\theta \in \omega$ for some set ω [1].

The traditional description of the EM algorithm consists of two steps:

E-step: Given the estimate from the previous iteration $\theta^{(m)}$, compute the conditional expectation:

$$Q(\theta / \theta^{(m)}) \tag{1}$$

M-step: The $(m+1)$-th guess of θ is:

$$\theta^{(m+1)} = \arg\max_{\theta \in \Omega} Q(\theta / \theta^{(m)}) \tag{2}$$

Since the E-step is only to compute the Q-function which is used in the M-step, EM can be summarized as just iteratively solving the M-step given by (2). When applying EM to a particular problem, this is usually the best way to think about EM because then time is not wasted for computing parts of the Q-function that do not depend on θ.

GENERALIZED NET MODEL OF THE EM ALGORITHM

The concept of Generalized nets (GNs) is introduced in [2 - 4]. Examples of constructed Generalized nets for data mining processes are presented in [1, 5 - 7]. In the present research, the GN of the Expectation-Maximization algorithm contains 8 transitions and 23 places (Fig. 1, on next page). The Generalized net consists of the following set of transitions:

$$A = \{Z_1, Z_2, Z_3, Z_4, Z_5, Z_6, Z_7, Z_8\},$$

where:

- Z_1 - "choosing observed data (y)";
- Z_2 - "choosing data for prediction (x)";
- Z_3 - "formulating the parametric density of y and x";
- Z_4 - "choosing a vector X for modelling the complete data";
- Z_5 - "formulating the aggregate parametric density of X and x";
- Z_6 - "making an initial estimation of $p(X'/ y, \theta^{(m)})$ ";
- Z_7 - "forming the conditional expected log-likelihood called Q-function";
- Z_8 - "check whether θ maximizes the Q-function";

α-token enters the GN via place L_1. The token has initial characteristic *"observed data"*. The token entering L_3 does not obtain any new characteristic. After the activation of transition Z_1, the α-token moves to place L_2 and obtains the following characteristic *"chosen observed data"*.

Transition Z_1 has the following form:

$$Z_1 = \langle \{L_1, L_3\}, \{L_2, L_3\}, R_1, \vee(L_1, L_3) \rangle,$$

where:

$$R_1 = \begin{array}{c|cc} & L_2 & L_3 \\ L_1 & false & true \\ L_3 & W_{3,2} & true \end{array}$$

and

$W_{3,2}$ = "the observed data is chosen".

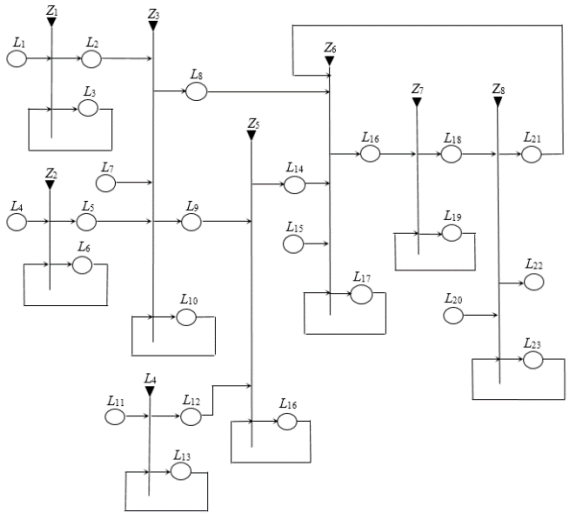

Fig. 1. GN model of EM algorithm

β-token enters the GN via place L_4 with initial characteristic "*data for prediction*". The token entering L_6 does not obtain any new characteristics. After the activation of transition Z_2, the β–token moves to place L_5 and obtains the following characteristic *"chosen data for prediction"*.

Transition Z_2 has the following form:

$$Z_2 = \langle \{L_4, L_6\}, \{L_5, L_6\}, R_2, \vee(L_4, L_6)\rangle,$$

where:

$$R_2 = \begin{array}{c|cc} & L_5 & L_6 \\ \hline L_4 & false & true \\ L_6 & W_{6,5} & true \end{array}$$

and

$W_{6,5}$ = "the data for prediction is chosen".

γ-token enters the GN via place L_7 with initial characteristic *"parameter to estimate"*. The tokens entering L_{10} do not obtain any new characteristics. After the activation of transition Z_3, the tokens from places L_2, L_5 and L_7 merge into two tokens (α_1 and β_1) in places L_8 and L_9 with characteristics, respectively, "*formed parametric density of the observed data*" and "*formed parametric density of the data for prediction*".

Transition Z_3 has the following form:

$$Z_3 = \langle \{L_2, L_5, L_7, L_{10}\}, \{L_8, L_9, L_{10}\}, R_3, \vee(\wedge (L_2, L_5, L_7), L_{10})\rangle,$$

where:

$$R_3 = \begin{array}{c|ccc} & L_8 & L_9 & L_{10} \\ \hline L_2 & false & false & true \\ L_5 & false & false & true \\ L_7 & false & false & true \\ L_{10} & W_{10,8} & W_{10,9} & true \end{array}$$

and

$W_{10,8}$ = "the parametric density $p(y/\theta)$ is formed";

$W_{10,8}$ = "the parametric density $p(x/\theta)$ is formed".

δ-token enters the GN via place L_{11} with initial characteristic *"random vectors"*. The token entering place L_{13} does not obtain any new characteristics. After the activation of transition Z_4, the δ-token moves to place L_{12} with the following characteristic *"chosen vector X"*.

Transition Z_4 has the following form:

$$Z_4 = \langle \{L_{11}, L_{13}\}, \{L_{12}, L_{13}\}, R_4, \vee(L_{11}, L_{13})\rangle,$$

where:

$$R_4 = \begin{array}{c|cc} & L_{12} & L_{13} \\ \hline L_{11} & false & true \\ L_{13} & W_{13,12} & true \end{array}$$

and

$W_{13,12}$ = "a vector X is chosen".

After the activation of transition Z_5, the tokens in places L_9 and L_{12} merge into one α_2-token in place L_{15} with characteristic "*formed aggregate parametric density* $p(X'/\theta)$ ". The tokens entering L_{16} do not obtain any new characteristics.

Transition Z_5 has the following form:

$$Z_5 = \langle \{L_9, L_{12}, L_{16}\}, \{L_{15}, L_{16}\}, R_5, \vee(\wedge (L_9, L_{12}), L_{16})\rangle,$$

where:

$$R_5 = \begin{array}{c|cc} & L_{14} & L_{16} \\ \hline L_9 & false & true \\ L_{12} & false & true \\ L_{16} & W_{16,15} & true \end{array}$$

and

$W_{16,15}$ = "the aggregate parametric density of X and x is formed, $p(X'/\theta)$ ".

ε-token enters the GN via position L_{15} with initial characteristic *"initial iteration"*. At the first activation of the transition, the tokens form places L_8, L_{14} and L_{15} merge into a new γ_1-token in place L_{16} with characteristic "*initial estimation of* $p(X'/y,\theta^{(m)})$ ". At the second activation of the transition, the tokens form places L_8, L_{14} and L_{15} merge into a new γ_2-token with characteristic *"next estimation of* $p(X'/y,\theta^{(m)})$ *"*. The tokens entering L_{17} do not obtain any new characteristics.

Transition Z_6 has the following form:

$$Z_6 = \langle \{L_8, L_{14}, L_{15}, L_{17}, L_{21}\}, \{L_{16}, L_{17}\}, R_6, \vee(\wedge (L_8, L_{14}\, L_{15}), L_{17}, L_{21})\rangle,$$

where:

$$R_6 = \begin{array}{c|cc} & L_{16} & L_{17} \\ \hline L_8 & false & true \\ L_{14} & false & true \\ L_{15} & false & true \\ L_{17} & W_{17,16} & true \\ L_{21} & false & true \end{array}$$

and

$W_{17,16}$ = "the first estimation of $p(X'/\, y, \theta^{(m)})$ is made".

After the activation of transition Z_7, the γ_1-token form place L_{16} moves to place L_{18} and obtains the following characteristic *"formed Q-function*". The token entering L_{19} does not obtain any new characteristics.

Transition Z_7 has the following form:

$Z_7 = \langle \{L_{16}, L_{19,}\}, \{L_{18}, L_{19}\}, R_7, \vee(L_{16}, L_{19})\rangle$,

where:

$$R_7 = \begin{array}{c|cc} & L_{18} & L_{19} \\ \hline L_{16} & false & true \\ L_{19} & W_{19,18} & true \end{array}$$

and

$W_{19,18}$ = "the Q-function is formed".

σ-token enters the GN via place L_{20} with initial characteristic "*criterion for maximization of the Q-function".* After the activation of transition Z_8, the tokens form places L_{18} and L_{20} move to place L_{21} or L_{22} depending on whether the criterion is met with characteristics respectively for L_{21} " $\| \theta^{(m+1)} - \theta^{(m)} \| \geq \mu$, *for some* $\mu > 0$" and " $\theta^{(m+1)} = \arg\max_{\theta \in \Omega} Q(\theta / \theta^{(m)})$ " for L_{22}. The tokens entering L_{23} do not obtain any new characteristics.

Transition Z_8 has the following form:

$Z_8 = \langle \{L_{18}, L_{20,} L_{23}\}, \{L_{21}, L_{22,} L_{23}\}, R_8, \vee(\wedge (L_{18}, L_{20}), L_{23})\rangle$,

where:

$$R_8 = \begin{array}{c|ccc} & L_{21} & L_{22} & L_{23} \\ \hline L_{18} & false & false & true \\ L_{20} & false & false & true \\ L_{23} & W_{23,21} & W_{23,22} & true \end{array}$$

and

$W_{23,21}$ = "the m-th estimate of θ is increased by 1";

$W_{23,22}$ = "a parameter θ which maximizes the Q-function is found".

CONCLUSION

The EM algorithm and its variants are regularly used to solve a broad range of today's estimation problems, from the multiple EM for motif elicitation algorithm for motif-finding in DNA sequences, to fitting mixture models to disambiguate targets from clutter in radar. The GN model presented in the current research shows how the EM algorithm works by splitting its two main steps into smaller ones and describing them in detail.

ACKNOWLEDGEMENT

The author is thankful for the support provided by "Application of intelligent methods for modelling and analysis of real processes" Project, Ref. No. NIH-499/2024, at Prof. Dr. Assen Zlatarov University, Burgas.

REFERENCES

1. Gupta, M., Y. Chen, Theory and Use of the EM Algorithm, Foundations and Trends in Signal Processing, **4**, No. 3 (2010), pp. 224-228.
2. Atanassov, K. Generalized Nets as a Tool for the Modelling of Data Mining Processes. -In: Innovative Issues in Intelligent Systems, **623**, (2016), pp. 161-215.
3. Atanassov, K., E. Sotirova, Generalized Nets, Prof. Marin Drinov Academic Publishing House, 2017.
4. Atanassov, K., On Generalized Nets Theory, Prof. M. Drinov Academic Publishing House, Sofia, 2007.
5. Bureva, V., E. Sotirova, K. Atanassov, Hierarchical generalized net model of the process of clustering, Issues in Intuitionistic Fuzzy Sets and Generalized Nets, Vol. 1, Warsaw School of Information Technology, (2014), pp.73-80.
6. Bureva, V., E. Sotirova, S. Popov, D. Mavrov, V. Traneva, Generalized Net of Cluster Analysis Process Using STING: A Statistical Information Grid Approach to Spatial Data Mining, London, 2017. Proceedings. Lecture Notes in Computer Science 10333, Springer.
7. Roeva O., T. Pencheva, A. Shannon, K. Atanassov, Generalized Nets in Artificial Intrelligence. Volume 7: Generalized Nets and Genetic Algorithms, Prof. Marin Drinov Academic Publishing House, 2013.

ANNUAL OF ASSEN ZLATAROV UNIVERSITY, BURGAS
BULGARIA, 2024, v. LIII(1)

APPLICATION OF ARTIFICIAL INTELLIGENCE IN MODERN WEB DEVELOPMENT

Todor Petkov, Plamen Stoyanov, Mehmed Mehmed
E-mail: todor_petkov@btu.bg

ABSTRACT

This article explores the transformative impact of Artificial Intelligence (AI) in web development. It begins by defining AI and outlining its historical evolution and current relevance in the tech industry. The theoretical part delves into key AI technologies such as machine learning, natural language processing (NLP), and computer vision, highlighting their roles in enhancing user experiences and improving website functionalities. In the program realization section, we provide a practical guide to integrating a chatbot into a website using popular tools such as TensorFlow.js, IBM Watson, and Microsoft Azure AI. The conclusion emphasizes AI's potential to revolutionize web development, encouraging further exploration and adoption of AI technologies.

Key words: *Artificial intelligence, web development*

INTRODUCTION

In the rapidly evolving digital era, web development stands as a cornerstone of the online presence of businesses, organizations, and individuals. The integration of Artificial Intelligence into web development is revolutionizing how websites are built, interacted with, and managed. AI technologies are not only enhancing user experiences but also streamlining the development process by automating repetitive tasks and offering advanced capabilities such as personalized content delivery, improved search functionalities, and intelligent customer support [1].

This article delves into the profound impact of AI on modern web development. It begins with a theoretical overview of AI and its applications in web development, highlighting the benefits these technologies bring. Following this, the article presents a practical guide to implementing AI in web development, focusing on integrating a chatbot into a website. This paper will demonstrate the seamless fusion of AI with web development, showcasing how these technologies can be leveraged to create more dynamic, responsive, and user-friendly websites. Through this exploration, a comprehensive understanding of AI's potential in transforming web development as well as practical insights into harnessing these technologies effectively will be gained.

OVERVIEW OF ARTIFICIAL INTELLIGENCE

Artificial Intelligence refers to the simulation of human intelligence processes by machines, particularly computer systems [2]. These processes include learning (the acquisition of information and rules for using the information), reasoning (using rules to reach approximate or definite conclusions), and self-correction [3]. AI encompasses a variety of technologies and methodologies, such as machine learning, deep learning, natural language processing, and computer vision, which enable machines to perform tasks that typically require human intelligence.

In the tech industry, AI is increasingly relevant due to its ability to enhance efficiency, improve decision-making, and provide more personalized user experiences. From virtual assistants and recommendation systems to autonomous vehicles and predictive analytics, AI is transforming how industries operate and interact with customers [4]. Its capacity to analyze vast amounts of data and derive insights that are beyond human capabilities makes it a pivotal tool in modern technology.

AI TECHNOLOGIES IN WEB DEVELOPMENT

1) Machine Learning

Machine learning (ML) is a core AI technol-

ogy that allows systems to learn from data and improve their performance without being explicitly programmed [5]. In web development, ML is used to analyze user behaviour, predict trends, and personalize content. For instance, recommendation engines on e-commerce sites and streaming platforms use ML algorithms to suggest products or media based on user preferences and past interactions.

2) Natural Language Processing (NLP)

Natural Language Processing (NLP) enables machines to understand, interpret, and respond to human language [6]. In web development, NLP powers chatbots, virtual assistants, and voice search functionalities, enhancing user interaction by providing immediate, context-aware responses. For example, customer support chatbots on websites use NLP to handle user queries efficiently, reducing the need for human intervention.

3) Computer Vision

Computer vision involves enabling machines to interpret and make decisions based on visual data [7]. This technology is used in web development for applications such as image recognition, facial recognition, and augmented reality. Websites that allow users to search for products using images, or social media platforms that automatically tag people in photos, utilize computer vision to improve user experience.

TOOLS AND FRAMEWORKS FOR AI IN WEB DEVELOPMENT

1) TensorFlow.js

TensorFlow.js is an open-source library that allows you to define, train, and run machine learning models entirely in the browser using JavaScript [8]. It is a versatile tool suitable for a wide range of tasks including real-time image recognition, natural language processing, and custom ML models.

- **Capabilities**: TensorFlow.js supports both the import of pre-trained models and the creation of new models from scratch. It leverages WebGL to accelerate computations, making it powerful enough for complex ML tasks.
- **Suitability**: Ideal for web developers looking to integrate advanced machine learning functionalities directly into their web applications without relying on server-side processing.

2) IBM Watson

IBM Watson offers a suite of AI services and APIs that can be integrated into web applications [9]. These services include Watson Assistant for building chatbots, Watson Natural Language Understanding for text analysis, and Watson Visual Recognition for image analysis.

- **Capabilities**: IBM Watson's services are highly scalable and robust, offering advanced AI functionalities such as sentiment analysis, language translation, and visual recognition.
- **Suitability**: Best suited for enterprise-level applications requiring sophisticated AI capabilities and high scalability.

3) Microsoft Azure AI

Microsoft Azure AI provides a range of AI services including Azure Cognitive Services, Azure Machine Learning, and Azure Bot Service [10]. These services allow developers to add AI functionalities such as speech recognition, image analysis, and predictive analytics to their applications.

USE CASE: CREATING AND INTEGRATING A CHATBOT INTO A WEBSITE

To create and integrate a chatbot into a website, the following steps are completed (all steps include free-use software):

1. Install Node.js;
2. Install Bootpress;
3. Create a new bootpress project by running the command: *bootpress init my-bot;*
4. Run the Botpress server to start developing your chatbot: *bootpress start;*
5. Define intents and responses by creating a JSON configuration file for “Welcome” intent:

```
{
  "version": "0.1.0",
  "flow": {
    "nodes": [
      {
        "id": "1",
        "name": "entry",
        "onEnter": [
          "say #!builtin_text-Welcome"
        ],
        "next": [
          {
            "condition": "true",
            "node": "2"
          }
]},
      {
        "id": "2",
```

```
      "name": "ask_name",
      "onEnter": [
        "say #!builtin_text-WhatIsYour-
Name"
      ],
      "next": []
    }],
  "startNode": "entry",
  "catchAll": {
    "onReceive": null,
    "next": []
  },
  "timeout": null
 }
};
```

6. Train the chatbot: Botpress automatically trains the chatbot based on the defined intents and responses;
7. Integrate the chatbot into a website: the proposed code is an HTML example of integration into a university website:

```
<!DOCTYPE html>
<html lang="en">
<head>
  <meta charset="UTF-8">
  <title>University Helper Chatbot</title>
</head>
<body>
  <h1>Welcome to Our University Web-
site</h1>
  <!-- Chatbot integration -->
  <iframe
    src="http://localhost:3000"
    width="400"
    height="600"
    style="border:none;">
  </iframe>
</body>
</html>
```

CONCLUSION

In conclusion, the integration of Artificial Intelligence in web development is profoundly transforming the digital landscape. AI technologies such as machine learning, natural language processing, and computer vision are revolutionizing how websites are built, interacted with, and managed. These technologies enhance user experiences by providing personalized content, improving search functionalities, and automating repetitive tasks, thus creating more dynamic, responsive, and user-friendly web applications.

The transformative potential of AI in web development cannot be overstated. As AI continues to evolve, its applications in web development will expand, offering even more innovative solutions to enhance functionality and user engagement.

Through the practical example of integrating a chatbot into a website, we have demonstrated how AI can be seamlessly incorporated into web projects using popular tools and frameworks like TensorFlow.js, IBM Watson, and Microsoft Azure AI. This example highlights the ease with which developers can adopt AI to enhance their web applications, making interactions more intuitive and efficient.

ACKNOWLEDGEMENT

The author is thankful for the support provided by “Application of intelligent methods for modelling and analysis of real processes” Project, Ref. No. NIH-499/2024, at Prof. Dr. Assen Zlatarov University, Burgas.

REFERENCES

1. Gobble, M., The Road to Artificial General Intelligence, Research Technology Management, **62**, 3, (2019), pp. 55-59.
2. Russell, S., P. Norvig, M. Chang. 1.1. What Is AI?. Section. In Artificial Intelligence a Modern Approach. 4th ed., Harlow: Pearson Education Limited. 2022.pp. 20-23.
3. Jean-Claude, K. A Comprehensive Overview of Artificial Intelligence. 2022, pp. 173-194.
4. Flasiński, M. Introduction to Artificial Intelligence, Textbook. Springer Nature. Switzerland. 2016.
5. Sarker, I.H. Machine Learning: Algorithms, Real-World Applications and Research Directions. SN COMPUT. SCI. 2. 160. 2021.
6. Khurana, D., A. Koli, K. Khatter, et al. Natural language processing: state of the art, current trends and challenges. Multimed Tools Appl, **82**, (2023), pp. 3713-3744.
7. Moin, T. Overview of Computer Vision. 2023, 10.13140/RG.2.2.13989.68327.
8. Pang, B., E. Nijkamp, Y. Wu. Deep Learning With TensorFlow: A Review. Journal of Educational and Behavioral Statistics, **45**, 2 (2020), pp. 227-248.
9. Chen, Y., JD. Argentinis, G. Weber. IBM Watson: How Cognitive Computing Can Be Applied to Big Data Challenges in Life Sciences Research, Clinical Therapeutics, **38**, 4 (2016), pp. 688-701.

10. Heller, M. Review: Microsoft Azure AI and Machine Learning aims for the enterprise. October 2021, online article (accessed 9/2024): https://www.infoworld.com/article/2261611/review-microsoft-azure-ai-and-machine-learning-aims-for-the-enterprise.html.

ANNUAL OF ASSEN ZLATAROV UNIVERSITY, BURGAS
BULGARIA, 2024, v. LIII(1)

RESEARCH OF OZONE AND NITROGEN DIOXIDE CONCENTRATIONS AND THE CURRENT PHOTOCHEMICAL PROCESSES IN THE ATMOSPHERIC AIR

Zdravka Nikolaeva, Maria Karabajakova
E-mail: z.v.burieva@gmail.com

ABSTRACT

An analysis was made of the impact of solar radiation on the average monthly concentrations of nitrogen dioxide and ozone in the atmosphere and the ongoing photochemical processes at the investigated four monitoring points (AMS Meden Rudnik, AMS Dolno Ezerovo, LV system *OPSIS and Mobile Station) of the Municipality of Burgas.*

The research shows that during the summer months, when solar radiation is strongest at midday, the concentration of nitrogen dioxide is the lowest and that of ozone is the highest. Ozone is formed primarily as a product of the breakdown of nitrogen dioxide under intense sunlight. This chemical process explains the higher monthly average concentrations of ozone, and the lower concentrations of nitrogen dioxide. Regarding the ozone in the ground air, it can be said that a clear reciprocity is observed in the change of the concentrations of ozone and nitrogen dioxide.

Key words: *air pollution, solar radiation, nitrogen dioxide, ozone, statistical processing, regression analysis, coefficient of determination, F-statistics*

INTRODUCTION

Studying the impact of solar radiation on some atmospheric pollutants and ongoing photochemical processes, as well as the formation of carcinogenic products, is an important problem related to the protection of the environment and life on Earth [1-4].

The protection of clean air [3] is one of the most important tasks and a fundamental duty of the entire society and is based on the principles of sustainable development. As a member of the European Union, Bulgaria has fully synchronized the air requirements with the European directives [5].

The country has a well-organized National System for Environmental Monitoring (NSEM), which monitors the quality of atmospheric air based on several indicators: total suspended dust, fine dust particles, heavy metals (lead, cadmium, nickel, arsenic), polyaromatic hydrocarbons, sulphur dioxide, nitrogen oxides, carbon monoxide, ozone, benzene, hydrogen sulphide. The Air Quality Index (AQI) for Burgas Municipality [7] is calculated on the basis of six of the controlled air pollutants: nitrogen dioxide, sulphur dioxide, particulate matter, hydrogen sulphide, ozone and styrene. However, the influence of atmospheric photochemical processes and the formed products on pollutant concentrations is not investigated and analyzed.

For the formation of tropospheric ozone, the following conditions must be present:

- presence of short-wave radiation ($\lambda \leq 410$ nm);
- the presence of nitrogen dioxide and the presence of methane, carbon monoxide or other inert molecules whose role is related to assisting the conversion of nitrogen monoxide into nitrogen dioxide.
- Under these conditions, nitrogen dioxide decomposes into nitrogen oxide and atomic oxygen, and atomic oxygen reacts with oxygen to form ozone. In principle, nitric oxide can react back with atomic oxygen to form the parent nitrogen dioxide, but because the presence of nitric oxide is a lot less than that of oxygen (21%), ozone is preferentially formed.

Recently, an important problem for the Municipality of Burgas has been the relatively high levels of ozone, which is why it is necessary to establish and model this important atmospheric pollutant for the city.

EXPERIMENT

In the present paper, data on the hourly average values of the concentrations of ozone and nitrogen dioxide in the atmosphere at four monitoring sites in the municipality of Burgas are taken on a

monthly basis [7]. There are the Automated measuring station (AMS) Meden Rudnik (European code BG0063A), AMS Dolno Ezerovo (European code BG0044A), LV system OPSIS (European code BG0056A) and a mobile station. The monthly average concentrations were calculated for the interval from 8 am to 5 pm local time, which covers the average minimal duration of solar irradiation.

The air quality index (AQI) is focused on the possible consequences on the human health which can appear within a couple of hours or days after breathing the polluted air. For the municipality of Burgas (http://air.burgas.bg), the AQI index is calculated using six air pollutants monitored: nitrogen dioxide, sulphur dioxide, particulate matter, hydrogen sulphide, ozone and styrene. The methods of the US Environment Protection Agency were used. [6, 8].

Table 1 shows the values of AQI, the corresponding requirements of the Standards for protection of human health and the colours used for visualization according to the definitions of the US EPA. AQI values higher than 300 indicate critical risks for human health and a high possibility for affecting the whole population.

Table 1. AQI values according to the US Environment protection agency

AQI values	Level of health risk	Colour
0 to 50	Good	Green
51 to 100	Moderate	Yellow
101 to 200	Unhealthy	Orange
> 200	Very unhealthy	Red

The AQI is defined by the formula [4]

$$x = \frac{a}{M}, \qquad (1)$$

where: a is measured concentration, $\mu g/m^3$ or mg/m^3; M is the allowable limit of human health protection for the same period. The values for SO_2, NO_2, O_3, H_2S and C_8H_8 are based on hourly average values and the PM-10 index is calculated by the method of 24 h floating average value.

For the calculation of the total solar radiation at the monitoring sites in the municipality of Burgas, data obtained from PVGIS-CMSAF were used [9]. The measured values cover a period of 12 years and the interval from 4.87 to 19.87 h at steps of 0.25 h.

The structure of the regression equation was as follows:

$$G = a_1 t + a_2 t^2 + a_3 t^3 + a_4 t^4 + a_5 t^5 + a_6 t^6 + b, \qquad (2)$$

where: G is total solar radiation per unit area per unit time, W/m^2; b, a_1, a_2, ..., a_6 are regression coefficients; t is time.

For estimation of the quality of the regression models, the coefficient of determination R^2 which determines the degree of linear dependence between the regresses involved in the model and the initial value was used. The significance of R^2 was checked using the Fisher criterion [8, 10]

$$F = \frac{R^2}{(1-R^2)} \cdot \frac{(N_1 - k)}{(k-1)}, \qquad (3)$$

where: k is number of the estimated parameters of the model; N_1 is the size of the sample of experimental data. The higher the calculated value of R^2, the more reliable the regression model is.

The aim of this paper is to present an analysis of the influence of the total solar radiation and the photochemical reactions on the monthly average concentrations of nitrogen dioxide and ozone in the atmosphere at the monitoring sites of the municipality of Burgas on a monthly basis.

RESULTS AND DISCUSSION

The changes of the monthly average concentrations of NO_2 and O_3 from 8 am to 5 pm (which is the average minimal monthly duration of solar radiation) for AMS Dolno Ezerovo are shown in Fig. 1.

It can be seen from the figures that during the summer months when the solar radiation is the strongest at noon, the nitrogen dioxide concentration has the lowest values while that of ozone has the highest ones. There is a clearly distinguishable reciprocity in the changes of the centration of nitrogen dioxide and ozone.

Ozone is formed mainly as a product of the decomposition of nitrogen dioxide under intense solar radiation. This photochemical process explains the higher monthly average concentrations of ozone and the lower monthly average concentrations of nitrogen dioxide.

The statistical estimations of the qualities of the models, e.g. AMS Dolno Ezerovo, are presented in Table 2.

The monthly models were estimated by the Fisher criterion. The available measured values of the total solar radiation, however, are different for the different months and they vary from 46 to 61.

Taking this into account, the parameters of the criterion of Fisher were determined to be as follows: $\alpha = 0.05$; $v_1 = 6$; $v_2 = 29 \div 54$.

Hence, the critical value: $F_{crit} = 2.27 \div 2.42$.

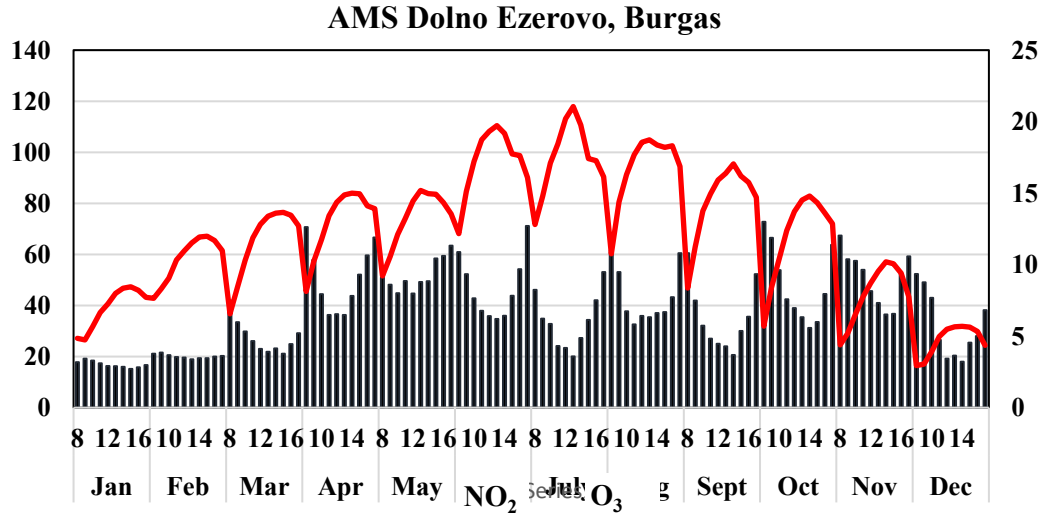

Fig. 1. Monthly average concentrations of NO_2 and O_3, AMS Dolno Ezerovo, 8 am – 5 pm

Table 2. AQI values according to the US Environment protection agency

Month	*Fisher coefficient, F*	R^2	Month	*Fisher coefficient, F*	R^2
January	5802.31	0.9988	July	4344.35	0.9974
February	1751.61	0.9951	August	3444.39	0.9970
March	2621.96	0.9964	September	2771.26	0.9965
April	2817.81	0.9964	October	2579.65	0.9966
May	3521.00	0.9968	November	2539.83	0.9969
June	3701.31	0.9969	December	2105.69	0.9964

Table 3. AQI, % and total solar radiation for the period from 11 am to 1 pm at AMS Dolno Ezerovo, Municipality of Burgas

Month	Time, h	AQI, %	G, W/m^2	Month	Time, h	AQI, %	G, W/m^2
	11	20.69	330.92		11	57.38	794.39
January	12	22.55	345.94	July	12	62.86	821.35
	13	24.86	324.99		13	65.51	784.51
	11	32.14	428.62		11	55.01	754.54
February	12	34.10	445.67	August	12	57.75	811.35
	13	35.85	422.78		13	58.26	744.51
	11	36.96	500.65		11	46.53	663.58
March	12	39.86	517.02	September	12	49.54	683.94
	13	41.64	495.89		13	50.98	655.19
	11	41.76	588.78		11	38.50	506.32
April	12	44.69	604.34	October	12	42.66	524.50
	13	46.26	582.89		13	45.16	499.71
	11	41.18	706.59		11	24.14	419.50
May	12	44.94	726.36	November	12	27.08	439.03
	13	47.26	697.76		13	29.68	411.86

	11	58.28	706.59		11	15.47	328.04
June	12	60.12	726.36	December	12	17.07	343.12
	13	61.36	697.76		13	17.58	323.05

As can be seen from Table 2, $F > F_{crit}$ and the coefficients of determination are quite close to unity. It means that the regression models are significant and can be used to predict the value of the total solar radiation.

Table 3 shows the AQIs calculated as percentage for the ozone at the AMS Dolno Ezerovo for the period from 11 am to 1 pm, as well as the values of the total solar radiation calculated according to formula (2). In Table 3, the AQI for ozone was calculated by formula (1) where: a is monthly average concentration of ozone, μg/m^3; M = 180 μg/m^3, Standard for protection of human health (SPHH) for a period of 1 h, Threshold for informing the population (TIP).

It can be seen from Table 3 that the level health hazard for the summer months is moderate, yellow, according to the classification of US EPA. Obviously, there is a relationship between the change of AQI for ozone and the total solar radiation. The AQI for the summer months is the highest which corresponds to the higher values of the total solar radiation. The highest average value of the AQI for ozone was found in July at 1 pm (65.51 %), while the lowest was in December (17.58 %).

The analysis of the influence of the total solar radiation on the monthly average concentrations of nitrogen dioxide and ozone in the atmosphere, resulting from the photochemical processes taking place, carried out for the monitoring sites of the municipality of Bourgas on a monthly basis clearly showed the relationship between the values of the total solar radiation and the concentration of ozone (AQI for ozone).

Ozone is one of the main air pollutants and, as far as practically all of it is generated by certain atmospheric processes (air quality index for ozone), its concentration is indicative of the degree of air pollution in the area.

CONCLUSIONS

An analysis was carried out of the influence of the total solar radiation on the monthly average concentrations of nitrogen dioxide and ozone at the monitoring sites of the Municipality of Burgas on a monthly basis.

In the summer months, when the solar radiation is the strongest at noon, the nitrogen dioxide concentration was the lowest, while that of ozone was the highest. There is a clearly distinguishable reciprocity between the changes of the concentrations of ozone and nitrogen dioxide.

Ozone is formed mainly as a result of the decomposition of nitrogen dioxide under intense solar radiation. This photochemical process explains the higher monthly average concentrations of ozone and the lower concentrations of nitrogen dioxide.

The quality of the regression models used to calculate the total solar radiation was estimated by the coefficient of determination R^2 and the criterion of Fisher. The coefficients of determination were very close to unity, which indicates that the regression models are adequate and can be used to predict the value of the total solar radiation.

It can be seen from the analysis carried out that there is a pronounced dependence between the AQI for ozone and the total solar radiation. AQI had the highest values for the summer months, which corresponds to the higher values of the total solar radiation.

Ozone is one of the main air pollutants and, as far as practically all of it is generated by certain atmospheric processes (air quality index for ozone), its concentration is indicative of the degree of air pollution in the area.

REFERENCES

1. Dimov, A. and P. Toromanova. Introduction to the Chemical and Metallurgical Technology and Ecology, Technics, Sofia, 1998.
2. Kutsarov. Air Pollution. Publishers Prof. Dr. Assen Zlatarov University, Burgas, (2001).
3. Air Act, Ministry of Environment and Water and Ministry of Health, last amended State Gazette, (5 July 2024).
4. Nikolova, N. Pollution and Monitoring of the Air. Pensoft, Sofia, (2008).
5. Ljubojev, N., J. Veselinovic and M. Dukic-Mijatovic. Protection of the Quality of Air in the Legislation of the Republic of Serbia as a Process of Harmonisation with the EU Legislation. Bulg. Oxid. Commun., **36**, 4 (2013), p. 1217.
6. Air Quality Index (AQI), A Guide to Air Quality and Your Health, US EPA, February

(2023), ttps://www.airnow.gov/publications/air-quality-index/air-quality-index-a-guide-to-air-quality-and-your-health/.
7. Air Quality in Burgas, Burgas Municipality (2023) http://air.burgas.bg.
8. System for training in statistics and statistical calculations with Microsoft Excel, (2021), https://www.btu.bg/statexcel/
9. Solar Radiation Databases (2020), http:// http://photovoltaic-software.com.
10. Dimitrova, R., J. Mihailova, Training System Statistics and Statistical Calculations with Excel (2020). http://teststat.hit.bg/.

ASSEN ZLATAROV UNIVERSITY
ANNUAL, Vol. LIII, BOOK 1, 2024
TECHNICAL AND NATURAL SCIENCES

Design and layout
Libra Scorp Publisher
www.meridian27.com

Printed in M&BM Ltd.
www.mbm-bg.com

Edition of
Assen Zlatarov University
www.btu.bg

ISSN 2603-3968

BURGAS, 2024

ISSN 2603-3968